https://doi.org/10.5194/egusphere-2026-3717
Preprint. Discussion started: 7 July 2026

Annual-resolution hydroclimate variability during the MCA–LIA transition in southern Iberia: insights into the role of cut-off lows (DANAs) from a speleothem record in Ardales Cave

Celia Campa-Bousoño[1], Miguel Iglesias[2], Iñaki Vadillo[3], Lucía Ojeda[3], Jorge Pisonero[4], Hai Cheng[5,6], R. Lawrence Edwards[7], Heather Stoll[8]

[1]Department of geology, University of Oviedo, Oviedo, 33005, Spain
[2]Vexiza, León, 24009, Spain
[3]Department of Geology, University of Malaga, 29071, Spain
[4]Department of Physics, University of Oviedo, Oviedo, 33005, Spain
[5]Institute of Global Environmental Change, Xi`an Jiaotong University, Xi`an, 710049, China
[6]Institute of Earth Environment, Chinese Academy of Sciences, Xi'an, 710049,China
[7]University of Minnesota, Minneapolis, MN, 55455, USA
[8]Department of Earth and Planetary Sciences, ETH, Zurich, 8092, Switzerland

Correspondence to: Celia Campa Bousoño (campacelia@uniovi.es) & Heather Stoll (heather.stoll@eaps.ethz.ch)

Abstract. High-resolution paleoclimate records from southern Iberia remain scarce, limiting the understanding of hydroclimatic variability during the transition from the Medieval Climate Anomaly (MCA) to the Little Ice Age (LIA). Here, we present an annually resolved multiproxy reconstruction based on the laminated Zerolín stalagmite from Ardales Cave, a climatically sensitive site influenced by both Atlantic and Mediterranean moisture sources. The chronology is constrained through the integration of U–Th dating, lamina counting, and color-based modelling. Hydroclimatic variability was investigated using a combined analysis of trace elements, stable isotopes, petrography, and forward geochemical modelling. The results reveal alternating humid and arid phases, with four major drought intervals (~1125, 1250, 1500, and 1560 CE) and wetter periods consistent with increased recharge and higher growth rates. Two additional intervals (1320–1450 and 1600–1700 CE) display increased variability and are interpreted as reflecting an increased influence of Mediterranean convective precipitation (cut-off lows) during transitional atmospheric conditions. At the regional scale, the main hydroclimatic phases are consistent with North Atlantic Oscillation variability, while these transitional periods show a weaker correspondence with large-scale Atlantic forcing. Overall, the record highlights the interplay between Atlantic and Mediterranean dynamics in shaping southern Iberian hydroclimate during the last millennium.

https://doi.org/10.5194/egusphere-2026-3717
Preprint. Discussion started: 7 July 2026

1 Introduction

Understanding the natural range of climate variability and contextualizing recent anthropogenic trends requires high-resolution paleoclimate reconstructions spanning the last millennium. This period includes major climatic phases such as the Medieval Climate Anomaly (MCA), the Little Ice Age (LIA), and the onset of the Industrial Period, which were characterized by complex and regionally variable shifts in temperature and precipitation patterns (Luterbacher et al., 2004; Mann et al., 2009; Neukom et al., 2019).

The Iberian Peninsula, located at the transition between the mid-latitude westerlies and subtropical circulation systems, is particularly suitable for reconstructing this variability. In the Mediterranean sector, hydroclimate fluctuations are strongly influenced by the North Atlantic Oscillation (NAO), which modulates temperature and precipitation at interannual to multidecadal timescales (Krichak & Alpert, 2005; Lionello et al., 2006; Suárez-Moreno et al., 2022). The alternation between Atlantic and Mediterranean air masses produces strong spatial gradients and seasonal contrasts in rainfall. Within this complex atmospheric setting, the southwestern and southeastern regions of the Iberian Peninsula are especially valuable for detecting hydroclimatic responses linked to NAO variability (Martín-Chivelet et al., 2011; Neves, 2025). Southeastern Iberia, in particular, is highly sensitive to the distribution and intensity of winter precipitation—the main hydrological input in this semi-arid region—making it especially responsive to large-scale atmospheric dynamics (García-Barrón et al., 2013; Morellón et al., 2011).

At the regional scale, Iberian hydroclimate variability is governed by the meridional migration and relative strength of the main North Atlantic meteorological agents (Azores High and Icelandic Low) and the associated westerly storm tracks (Trigo et al., 2018; Simons, 2022; Hakam et al., 2025). This large-scale setting, together with the peninsula's pronounced orographic variability, generates sharp spatial gradients and a complex mosaic of microclimates within less than 1000 km—from the humid, Atlantic-dominated regions of the northwest (e.g., Galicia) to the semi-arid Mediterranean basins of the southeast (e.g., Almería or Murcia) (Beguería et al., 2023; Gonzalez-Hidalgo et al., 2024). These contrasts imply that even nearby paleoclimate archives may record different expressions of the same large-scale forcing, underscoring the need for hydroclimatically sensitive sites capable of resolving regional differences (Beguería et al., 2023; Gonzalez-Hidalgo et al., 2024).

Despite its climatic sensitivity, few high-resolution paleoclimate archives from southern Iberia combine robust chronologies with sub-annual resolution. Existing lacustrine and marine reconstructions (e.g., Martín-Puertas et al., 2010; Rodrigo-Gámiz et al., 2022) have provided valuable insights into long-term variability but often lack the temporal precision required to resolve short-term hydroclimatic changes. This limitation underscores the importance of developing new high-resolution records capable of capturing seasonal to interannual variability.

Speleothems constitute one of the most suitable archives for this purpose, particularly when they preserve continuous annual laminae that can be precisely dated. The laminated records from caves allow true seasonal-to-annual reconstructions based on lamina counting and U–Th dating (Baker et al., 2008; Frisia et al., 2005; Nuriel et al., 2021; Tan et al., 2003). Speleothems with well-defined laminae have shown strong coherence with instrumental and historical data in regions with pronounced

https://doi.org/10.5194/egusphere-2026-3717
Preprint. Discussion started: 7 July 2026

seasonality (Bini et al., 2020; Voarintsoa et al., 2017), yet they remain scarce in the western Mediterranean, particularly in continental southern Spain. Recent advances in the central Pyrenees (Bartolomé et al., 2024) and Menorca (Cisneros et al., 2024) have provided important new information on hydroclimatic variability over the last millennium, though these records still lack the seasonal resolution necessary to characterize short-term fluctuations and transitional intervals, such as between the end of the MCA and the onset of the LIA. Understanding this MCA–LIA transition is particularly relevant, as it marks a period of profound reorganization in the North Atlantic–Mediterranean atmospheric circulation. This interval involved major shifts in large-scale pressure systems and jet-stream dynamics, including increased blocking frequency and enhanced meridional flow, which likely amplified the alternation between prolonged droughts and episodes of torrential precipitation.

Against this background, the Zerolín stalagmite from Ardales cave (Málaga, southern Spain) provides an exceptional opportunity to reconstruct short-term hydroclimatic variability during one of the most unstable phases of the last millennium. The site lies in a region influenced by both Atlantic and Mediterranean air masses and receives most of its recharge from winter precipitation. Its position between the Sierra de las Nieves and the Sierra de Grazalema enhances its sensitivity to seasonal contrasts in moisture sources, as these mountain ranges intercept Atlantic fronts and generate steep precipitation gradients over short distances. This geomorphological context, combined with the stalagmite's exceptionally well-preserved annual laminae and rapid growth rate, enables the construction of a robust, annually resolved chronology based on U–Th dating, lamina counting, and color banding analysis.

Hydrologically, the Ardales karst system is recharged mainly by winter and spring precipitation under Atlantic influence, whereas summer and autumn rainfall is less frequent but can be extreme and is often linked to cut-off lows, providing an additional Mediterranean contribution to infiltration (Halifa-Marin et al., 2021; Perez & García, 2023; Martinez-Artigas et al., 2021; Miró et al., 2022). This seasonal duality makes the site particularly well-suited to capture variability in the relative contribution of Atlantic vs. Mediterranean hydroclimatic regimes.

To explore hydroclimate variability at seasonal to interannual scales, this study applies a multiproxy approach that integrates stable isotopes (eg., $\delta^{13}C$), trace-element ratios (eg., Mg/Ca), and petrographic features to investigate the processes controlling speleothem deposition. The interpretation of geochemical variations is supported by modern cave monitoring, including dripwater chemistry and cave-air pCO_2 measurements, which inform on infiltration dynamics, Prior Calcite Precipitation (PCP), and ventilation processes (Fairchild et al., 2001; Sinclair et al., 2012; Treble et al., 2003). Linking these geochemical indicators to the regional atmospheric framework allows the identification of specific hydroclimatic mechanisms, such as prolonged summer–autumn droughts and episodic Mediterranean convective events (in Spanish "Depresión Aislada en Niveles Altos", or DANA).

Furthermore, the I-STAL forward model (Stoll et al., 2012) is used to assess how hydrological extremes are recorded in speleothem geochemistry and to evaluate their influence on potential growth hiatuses. The analysis also explores multiannual periodicities in trace-element data and their possible relationship with NAO variability, providing new insights into the extent to which large-scale atmospheric patterns modulate hydroclimatic conditions in the western Mediterranean.

https://doi.org/10.5194/egusphere-2026-3717
Preprint. Discussion started: 7 July 2026

By combining annually laminated speleothem data from southern Iberia with modern cave monitoring and numerical modeling, this study offers the annual-scale resolution necessary to capture hydroclimatic variability during the MCA–LIA transition. It thus addresses a key temporal gap in existing Mediterranean records and contributes to a better understanding of the coupling between atmospheric circulation, karst hydrology, and speleothem geochemistry, refining the regional expression of large-scale climate variability in the western Mediterranean.

2 Study sites

2.1 Cave location and temperature

Ardales Cave (UTM: 337.110/4.082.540; 565 m a.s.l.) is located near the village of Ardales (Málaga province, southern Spain), on the northern slope of Calinoria Hill, ~50 km from the Mediterranean coast and close to the confluence of the Turón, Guadalteba, and Guadalhorce river basins. The entrance, situated at the base of a steep Pleistocene sediment cone, provides access to ~1577 m of passages (~1394 m in horizontal projection) with a vertical range of ~35 m (Fig. 1). The system comprises large chambers, phreatic conduits, and collapsed zones, organized into three principal levels: the Upper Galleries (-16 m), the Lower Galleries (-23 m), and the Collapse Rooms (+7 to -24 m), reflecting progressive lowering of the water table during cave development (Ramos et al., 2014). The Upper Galleries, discovered in 1981 and closed to visitors, remain in pristine condition and host the speleothem analyzed in this study.

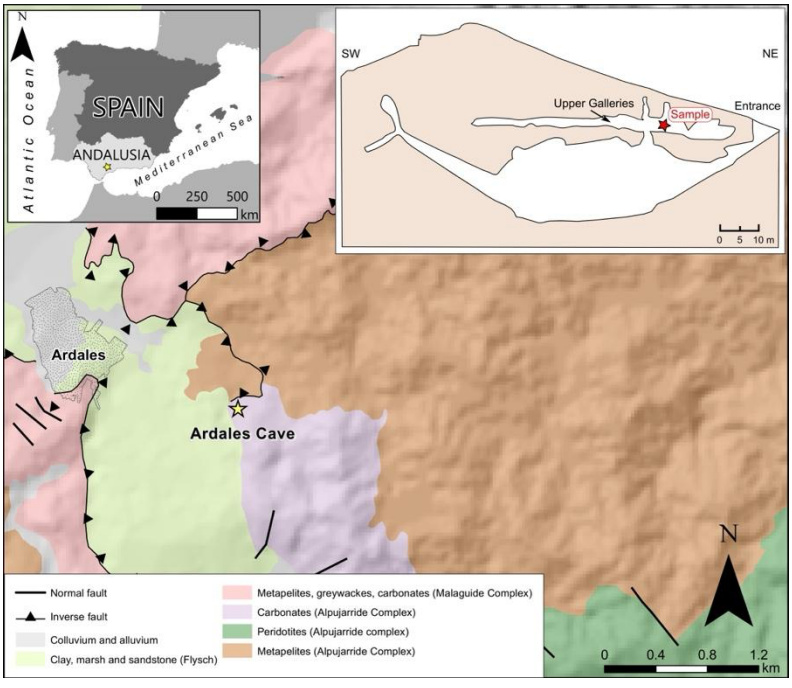

https://doi.org/10.5194/egusphere-2026-3717
Preprint. Discussion started: 7 July 2026

Figure 1. Location and geological context of Ardales Cave, showing the position of the Zerolín stalagmite. Geological map showing the main lithological units of the area. The yellow star indicates the location of Ardales Cave. The inset shows the Upper Galleries and the position of the Zerolín stalagmite (red star).

The cave microclimate is characterized by remarkable thermal stability, with a mean annual temperature of ~17 °C (Fernandez-Cortes et al., 2022). Seasonal ventilation is limited. In winter, a cold-air plug forms at the entrance, strongly restricting exchange with the exterior and promoting CO_2 accumulation, while in summer ventilation increases. As a result, internal CO_2 concentrations vary from ~600 ppm in summer to ~1500 ppm in winter (Cantalejo, 2013; Fernandez-Cortes et al., 2022). The relative isolation and stability of the Upper Galleries favor near-equilibrium conditions and long-term preservation of paleoclimate archives.

2.2 Geology and vegetation

Ardales Cave lies within the Subbetic zone of the External Betic Cordillera, although the host rocks belong to the Alpujárride Complex of the Internal Zone (Fig. 1). The cave formed within the Bonella–Capellán Unit, composed of metamorphic Triassic dolomitic marbles at the base and Jurassic limestones with interbedded chert at the top. Lithological variability has influenced both morphology and hydrology: while carbonate dissolution dominates most sectors, zones with exposed insoluble metapelites evolved mainly through mechanical collapse. Karstification initiated between the Late Miocene and Early Pleistocene during major tectonic uplift, with the main speleogenetic phases occurring between the Upper Pliocene and Middle Pleistocene. Collapse chambers developed subsequently during the Late Pleistocene (Ramos et al., 2014).

The regional climate is Mediterranean (Csa; Peel et al., 2007), characterized by hot, dry summers (mean temperature ~24.5°C, June–September) and mild, wet winters (mean temperature ~11.0°C, November–March). Precipitation is highly seasonal, peaking in November–December (~100 mm month^{-1}), and nearly absent during summer (<1 mm month^{-1}). Vegetation surrounding the cave is dominated by Mediterranean sclerophyllous woodland, primarily holm oak (*Quercus ilex*), adapted to summer drought and recurrent wildfires. Associated shrub species include *Thymus baeticus, Phlomis purpurea, Smilax aspera*, and *Pistacia lentiscus* (Rivas-Martínez et al., 2001). Soils consist of terra rossa, Mediterranean red soils, and acidic brown soils. On the summit of Calinoria Hill, vegetation cover is sparse, with rocky outcrops and scattered shrubs; in some cases, holm oaks root deeply enough to reach the Upper Galleries. According to the bioclimatic zonation of Rivas-Martínez (1987), the site belongs to the lower Mesomediterranean belt.

3 Methods

3.1 Speleothem samples

This study is based on a laminated stalagmite (Zerolin) recovered from the restricted Upper Galleries of Ardales Cave (southern Spain, Fig. 1). The speleothem was collected following strict conservation protocols due to the presence of prehistoric cave art

https://doi.org/10.5194/egusphere-2026-3717
Preprint. Discussion started: 7 July 2026

in the vicinity. The specimen displays continuous growth layers characterized by the alternation of light, porous laminae and dark, compact laminae. The stalagmite has a total length of 580 mm. From the top of the stalagmite (defined as 0 mm) down to 100 mm, the alternation between light and dark laminae progressively fades, whereas a well-defined lamination is preserved in the basal zone. Accordingly, this study focuses on the interval between 580 and 100 mm from the top, where the laminae are continuous and suitable for high-resolution analyses.

Prior to sampling, detailed field campaigns were conducted in 2016 and 2018 to assess the cave environment and its surrounding vegetation and soil properties, as well as to collect drip water samples during contrasting hydrological periods (dry and wet seasons) together with regional meteorological data (AEMET). These samples were used to characterize the modern hydrogeochemical system feeding the speleothem.

After extraction, the stalagmite was cut parallel to the growth axis using a diamond saw, producing two symmetrical halves. The inner growth axis was polished and prepared for high-resolution imaging and microdrilling. The sample was analyzed for mineralogical integrity using petrographic thin sections to assess the preservation of closed-system behavior. All geochemical sampling was conducted along the central axis to ensure the highest spatial and temporal resolution.

3.2 Age model

The age model was built using both U/Th dating and lamina counting. Powdered samples for U/Th dating were drilled with a precision Sherline 5400 microdrill along the growth axis, using tungsten carbide drill bits of 2.5 mm diameter for isotope analysis. All drilling was conducted under laminar flow hoods to avoid contamination, with cleaning protocols using 2% HNO_3 and ethanol between samples. U/Th ages were determined using methods described in Stoll et al. (2015). Details of dates, corrected initial $\delta^{13}U$ ratios and U contents of the samples were published previously (Campa-Bousoño et al., 2021).

The resulting age–depth model was constructed using the Bayesian Bchron software package (Haslett & Parnell, 2008; Parnell et al., 2008), which generates 1000 age ensembles that incorporate dating uncertainties and allow the identification of possible growth hiatuses. To complement this approach, optical imaging of polished stalagmite surfaces was carried out to identify and count laminae, which were verified against absolute dates using the WinGeol Lamination Tool (Meyer et al., 2006). Laminar counting relied on a high-resolution image montage calibrated at ~20 µm/pixel, with a detectability threshold of ~80 µm (~4 px) applied to ensure that only resolvable laminae were considered. To quantify the per-lamina miscount probability p, three representative segments along the growth axis were inspected, and laminae thinner than 8 µm were classified as below detectability. The pooled value of p was then defined as the fraction of below-threshold laminae across all segments. Random counting uncertainty for cumulative lamina counts N(d) at depth dd was propagated with a binomial model, Eq. (1), and 95 % confidence intervals were calculated assuming annual lamination. Where such annual laminations were confirmed, they were integrated into the Bayesian age model to refine temporal resolution.

$$\sigma_N(d) = \sqrt{N(d)\, p\, [1-p]}, \quad (1)$$

https://doi.org/10.5194/egusphere-2026-3717
Preprint. Discussion started: 7 July 2026

3.3 Trace-element and stable isotope analyses

Trace-element concentrations were measured using both solution-based and laser ablation techniques. For low-resolution analyses, powder samples were collected at 1 mm intervals along the entire 500 mm-long basal speleothem. These samples (1-300 mg) were dissolved in 2% HNO_3 (Tracepur) and analyzed using a Thermo ICAP DUO 6300 ICP-OES at the University of Oviedo, following the procedure described by de Villiers et al. (2002), allowing the quantification of major and trace elements.

To obtain high-resolution geochemical data, a 23 mm basal segment of the speleothem (from 317 to 340 mm) was selected. This portion was chosen due to its well-defined lamination and the availability of a U/Th age constraint in close proximity, making it particularly suitable for detailed analyses. Within this section, samples were extracted every 0.2 mm using a Sherline micromill, resulting in a continuous trench approximately 3 mm wide along the growth axis. The resulting powders were analyzed at ETH Zurich using an Agilent 8800 triple quadrupole ICP-MS. In parallel, Laser Ablation ICP-MS analyses were performed on polished thick sections using a Photon Machines Analyte G2 excimer laser coupled to an Agilent 7700cx ICP-MS, achieving a spatial resolution of approximately 20 µm. Both analytical techniques followed standard calibration protocols (Gagnon et al., 2008; Müller et al., 2009).

Stable isotope analyses ($\delta^{13}C$ and $\delta^{18}O$) were performed on micromilled carbonate powders collected at 2 mm resolution along the entire stalagmite and at 0.2 mm within the high-resolution basal segment (317-340 mm). Analyses were carried out using two isotope ratio mass spectrometers: a ThermoFisher Delta V IRMS with GasBench II interface at ETH Zurich for the high-resolution samples, and a Nu Instruments Horizon IRMS with GasPrep system at the University of Oviedo for the lower-resolution transect. Carbonate powders (~200 µg) were reacted with phosphoric acid under helium atmosphere and analyzed relative to VPDB using international and in-house standards. The analytical precision was estimated based on repeated measurements of reference materials, yielding reproducibility values below ±0.1‰ for both $\delta^{18}O$ and $\delta^{13}C$. Analytical procedures followed the method described by Breitenbach & Bernasconi (2011) and Stoll et al. (2015).

3.4 Data analysis and geochemical modeling

All statistical analyses were performed using R and SPSS v20. Principal Component Analysis (PCA) was used to identify the dominant geochemical processes affecting trace-element variability, with factor extraction based on eigenvalues >1 and varimax rotation. Correlations between proxies were assessed using Pearson's r. ANOVA tests were applied to evaluate the influence of lamina color on geochemical composition, where η^2 was used as a measure of effect size in ANOVA. Time-series analyses included cross-wavelet and wavelet coherence methods (Grinsted et al., 2004; Torrence & Compo, 1998), allowing identification of shared variability and phase relationships between geochemical proxies. All wavelet analyses were conducted using Monte Carlo simulations to assess statistical significance. Analyses were performed separately for the LA-ICP-MS dataset and the solution-based dataset.

https://doi.org/10.5194/egusphere-2026-3717
Preprint. Discussion started: 7 July 2026

To further assess the role of degassing and PCP in modifying trace-element signals, the I-STAL model (Stoll et al., 2012) was applied to estimate the drip interval thresholds, CO_2 concentration, and cave temperature compatible with calcite precipitation, based on the observed Mg/Ca and Sr/Ca ratios. In addition, maximum and minimum Mg/Ca and Sr/Ca values from the speleothem were used to back-calculate plausible dripwater compositions, which were then compared to modern dripwater data collected during wet and dry seasons. These reconstructed dripwater values were further evaluated using experimentally derived partition coefficients (e.g., Day & Henderson, 2013; Fairchild et al., 2010; Gascoyne, 1983; Rossi & Lozano, 2016; Tremaine & Froelich, 2013), allowing assessment of whether modern extremes have analogs in the recent past, and whether differences in partitioning or karst functioning may explain their absence from the speleothem record. These drip water analyses can be consulted in Appendix A.

4 Results

4.1 Speleothem description and petrography

The studied stalagmite, Zerolín, is a 580 mm long conical speleothem retrieved from the Upper Galleries of Ardales Cave. It displays clear visual lamination and marked color variation along its growth axis (Fig. 2). From the base to ~100 mm from the top, the stalagmite exhibits alternating opaque white (~3 µm thick) and translucent dark (~1 µm thick) laminae. Also, although it is not part of this study, between 100 to the top, this lamination disappears within a compact translucent yellowish zone, followed by a pale grey section with very weak layering. The basal portion has a diameter of ~10 cm, gradually tapering to ~4 cm near the apex. Lamination becomes increasingly subdued towards the uppermost part, which also shows a darker hue. Petrographic analysis reveals that the opaque white laminae are porous and exhibit an open columnar texture, while the translucent dark laminae are denser and correspond to a compact columnar texture (Fairchild & Baker, 2012; Frisia, 2015; Frisia et al., 2000).

https://doi.org/10.5194/egusphere-2026-3717
Preprint. Discussion started: 7 July 2026

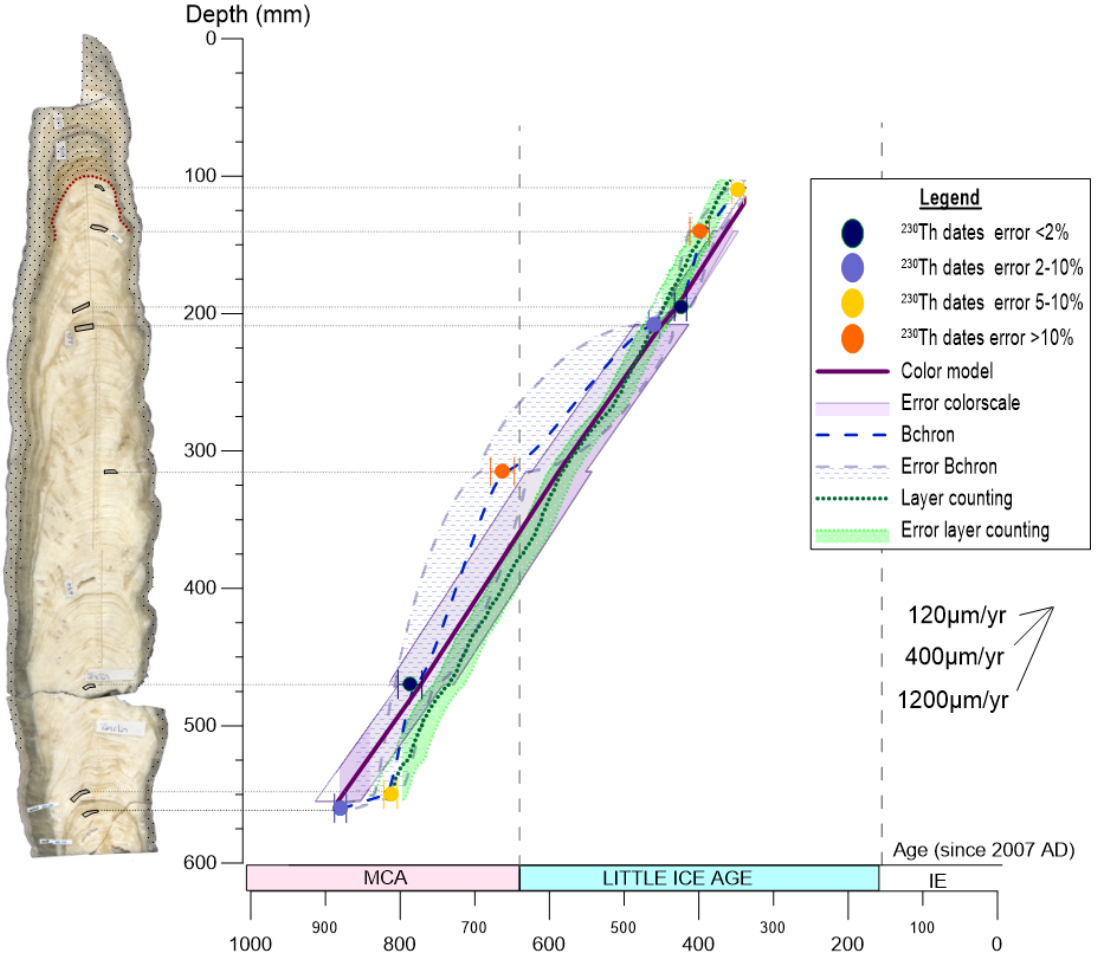

Figure 2. Age–depth model and corresponding growth rate (slope) for the zone characterized by continuous light–dark lamina alternation in the Zerolín speleothem. On the far left, the original speleothem image is shown with depth expressed in centimeters along the Y-axis. The dotted area marks the section where the annual lamina alternation is discontinuous and therefore excluded from the study, while the red line indicates the boundary where annual resolution is lost. U–Th dates are plotted directly on the speleothem image; warmer colors indicate greater deviation from the modeled color-based ages (Campa-Bousoño et al., 2021). Three age models are represented: the blue dashed line corresponds to the Bchron model, the green dashed line to the lamina-counting model, and the purple continuous line to the color-based model. The approximate growth rate, as derived from the slope of each age model, is shown on the right-hand side of the graph.

These microtextures were confirmed via petrographic thin sections (Fig. 3). The speleothem was still active at the time of collection, as evidenced by subsequent calcite crystal growth on the broken surface during post-sampling visits.

https://doi.org/10.5194/egusphere-2026-3717
Preprint. Discussion started: 7 July 2026

The stalagmite formed under relatively undisturbed conditions in a sector of the cave isolated from human influence. Dripwater feeding Zerolín emanates from a large, overhanging stalactite aligned along a major dolomitic fracture, suggesting that water infiltration has a substantial epikarst residence time and a well-defined flow path.

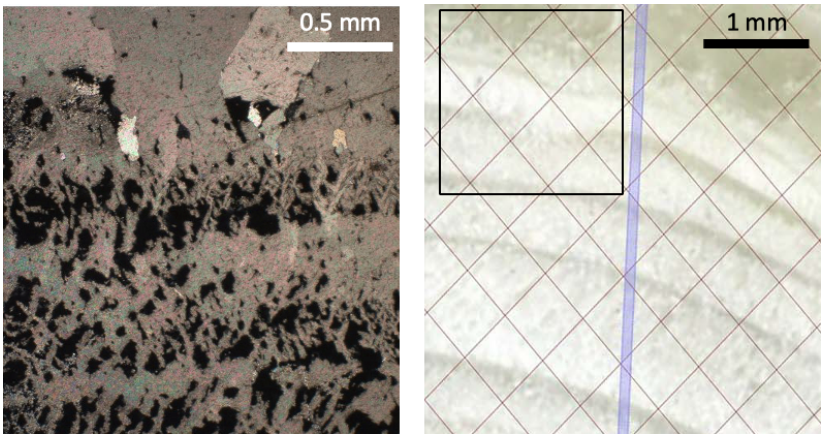

Figure 3. Macroscopic and microscopic views of the growth layers in the speleothem. The image on the left shows a photomicrograph of a thin section of the speleothem under crossed Nicols, taken with a Zeiss Axioscope digital camera at 2.5× magnification. The white (light) laminae display notable porosity. The image on the right presents the polished surface of the speleothem, where alternating light and dark laminae are visible. A 1 mm scale and a red spatial grid are included for reference. The black square marks the sector corresponding to the thin section shown on the left.

4.2 Chronology and lamina counting

The age model for Zerolín combines U/Th dating with optical lamina counting. In the basal section of the stalagmite, counting performed with the WinGeol Lamination Tool reveals highly regular alternations of light and dark laminae, indicating an average growth rate of approximately 800 µm/yr. From this counting, the associated error was also evaluated: across the three analyzed segments, 165 laminae were examined, of which 30 were thinner than 80µm. These sub-threshold laminae yielded a pooled per-lamina miscount probability of $\hat{p}$=0.182 (95% CI: 0.123–0.241), which was directly incorporated to propagate uncertainty in the chronological estimation.

Independently, the Bayesian age model constructed with Bchron from U/Th dates showed results consistent with the lamina counting, reinforcing the reliability of both approaches. Finally, to further assess the robustness of the chronology, growth rates derived from lamina counting were compared with those obtained from the color-index age model (Campa-Bousoño et al., 2021). In the laminated sector, both methods yielded consistent results (Fig. 2), confirming the robustness of the proposed age model.

https://doi.org/10.5194/egusphere-2026-3717
Preprint. Discussion started: 7 July 2026

4.3 Trace element ratios and isotope variability in the rapid-growth sector

A high-resolution geochemical transect was conducted on a 20 mm segment of the basal zone of the Zerolín speleothem (317–340 mm from the top), corresponding to a period of rapid growth. Comparison between techniques shows that although general trends are consistent, absolute concentrations differ substantially for certain elements. Detrital and colloidal elements values up to 400 % higher in LA-ICP-MS measurements compared to solution-based analyses, due to the presence of poorly soluble fractions not dissolved by weak nitric acid. This contrast is especially evident in these elements like Al/Ca and Y/Ca. In contrast, Mg/Ca and Sr/Ca ratios exhibited closer agreement between both analytical methods (Fig. 4).

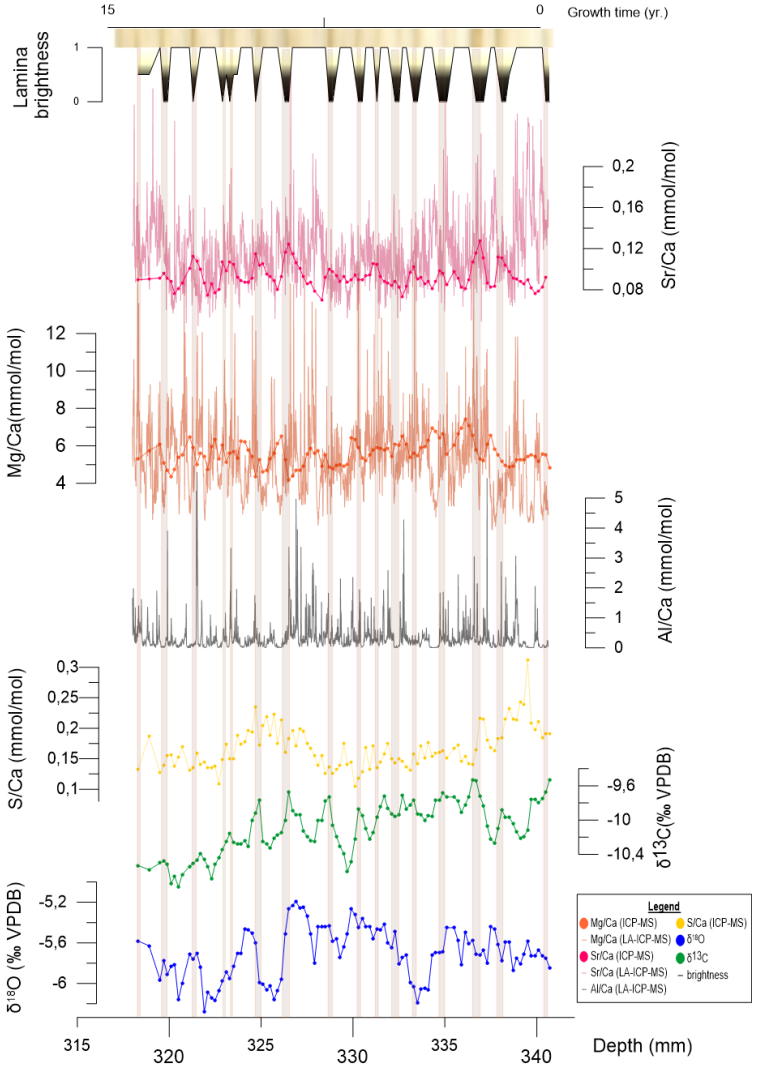

Figure 4. Graph showing the variation in coloration and geochemical proxies relative to distance (in mm) from the top of the speleothem. Trace-element ratios (Mg/Ca, Sr/Ca, Al/Ca, and S/Ca) were measured using LA-ICP-MS-Q, except for S/Ca,

https://doi.org/10.5194/egusphere-2026-3717
Preprint. Discussion started: 7 July 2026

which was determined exclusively by ICP-MS-QQQ after acid digestion. Stable isotopes ($\delta^{18}O$ and $\delta^{13}C$) were analyzed using GB-IRMS. At the top, a high-resolution image of the laminated section is shown together with an approximate estimate of elapsed years based on the counting of light–dark lamina pairs. Lamina brightness values are included as a conceptual visual model, where 1 represents light laminae and 0 represents dark ones, to illustrate brightness variation along the profile. Brown rectangles indicate reference values corresponding to the dark-colored laminae.

Pearson correlation matrices (Table A2, Appendix A) reveal significant positive correlations among Al/Ca, Y/Ca, Cu/Ca, Zn/Ca, and Pb/Ca in the LA-ICP-MS dataset, consistent with their association to insoluble or colloidal phases. In the solution dataset, Sr/Ca and Ba/Ca show a strong positive correlation, while Sr/Ca and Mg/Ca exhibit a negative correlation (Table 1). Mg/Ca also shows moderate to high correlation with Al/Ca in both datasets.

	Mg	Al	P	S	As	Sr	Y	Ba	U	$\delta^{18}O$	$\delta^{13}C$
Mg	1	**0.254***	-0.029	**–0.282***	0.100	**-0.261***	-0.12	0.102	0.089	-0.054	0.174
Al		1	-0.211	-0.113	0.115	0.071	-0.245	0.019	-0.106	-0.218	-0.200
P			1	**0.459****	0.115	**-0.358****	**0.570****	**-0.328****	0.245	-0.042	-0.03
S				1	**0.325****	0.164	**0.423****	-0.210	-0.13	0.004	0.167
As					1	0.019	0.199	**-0.252****	-0.123	-0,124	0.047
Sr						1	**-0.465****	**0.499****	**-0.501****	0.151	0.211
Y							1	**-0.256***	**0.444****	-0.203*	-0.151
Ba								1	0.044	0.07	**0.269***
U									1	-0.148	0.024
$\delta^{18}O$										1	**0.292****
$\delta^{13}C$											1

Table 1. Pearson correlation coefficients between stable isotopes and trace elements analyzed (solution method). Values marked with * are significant at $p < .05$; those marked with ** are significant at $p < .01$. Values highger than +-.25 are highglihted in bold for easy identification.

Stable isotope data in this high-resolution area display only weak correlations with trace-element ratios. A moderate positive correlation was observed between $\delta^{13}C$ and $\delta^{18}O$, but neither isotope shows significant correlation with Mg/Ca, Sr/Ca, or other trace elements (Table 1). Absolute values of $\delta^{13}C$ ranged from -10.8 to -9.5 ‰, and $\delta^{18}O$ from -6.2 to -5.2 ‰ (Fig. 4).

4.4 Principal Component Analysis (PCA) and geochemical controls

To explore major geochemical patterns and identify the dominant processes affecting the trace-element and stable isotope composition of the speleothem, a PCA was conducted on data from the rapid-growth sector.

https://doi.org/10.5194/egusphere-2026-3717
Preprint. Discussion started: 7 July 2026

The first three principal components explain over 55 % of the total variance in both datasets. PC1 (~30 %) is characterized by high loadings of Pb/Ca, U/Ca, and Zn/Ca in the LA-ICP-MS data, and Ba/Ca and Sr/Ca (positive) versus Y/Ca and P/Ca (negative) in the solution data, reflecting variability related to the incorporation of colloidal or detrital material.

PC2 (~17 %) shows positive contributions from Mg/Ca and negative from Sr/Ca and Ba/Ca in the LA-ICP-MS dataset. In solution data, Mg/Ca and U/Ca load positively, while S/Ca and Sr/Ca load negatively. This component captures variations associated with degassing and PCP, growth rate, and water-rock interaction.

PC3 (~12 %) is influenced by Y, U, and Pb (positive) and Sr/Ca, Zn/Ca, and Cu/Ca (negative) in the LA-ICP-MS data. In the solution dataset, $\delta^{13}C$ and $\delta^{18}O$ load negatively, indicating potential seasonal variations linked to hydrological and atmospheric conditions.

A summary of loadings and scores for the three components is shown in Fig. 5 and Fig. A3 (Appendix A).

https://doi.org/10.5194/egusphere-2026-3717
Preprint. Discussion started: 7 July 2026

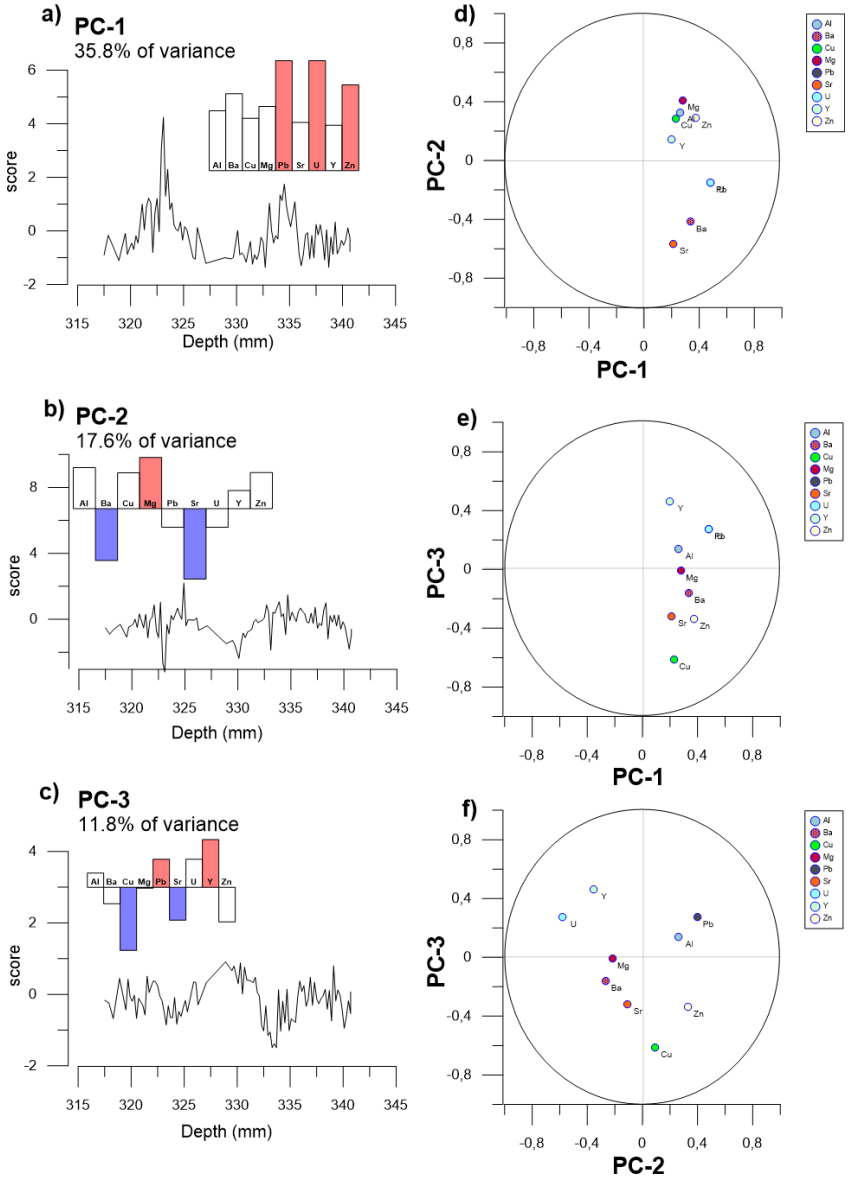

Figure 5. PCA of nine trace elements measured by LA-ICP-MS (27Al, 138Ba, 65Cu, 25Mg, 208Pb, 88Sr, 238U, 89Y, 66Zn) along the annually laminated section of the speleothem. Panels A-C show PCA scores for the first three components plotted against distance from the top. Panels D-F represent variable loadings for PC2 vs. PC1, PC3 vs. PC1, and PC3 vs. PC2. Loadings are color-coded to indicate the strength and direction of association (red = positive, blue = negative), and unit circles define the theoretical bounds of variable influence.

https://doi.org/10.5194/egusphere-2026-3717
Preprint. Discussion started: 7 July 2026

4.5 Wavelet periodicities and geochemical records

Wavelet analysis of the high-resolution LA-ICP-MS data (Mg/Ca, Sr/Ca, Al/Ca, Ba/Ca) from the laminated basal section of the Zerolín speleothem revealed significant periodicities at approximately 0.8, 1.6, and 4 mm along the growth axis (Fig. 6). The ~0.8 mm signal, interpreted as an annual cycle based on the estimated average growth rate of ~800 µm/year, was most prominent in the Mg/Ca ratios, while Sr/Ca, Ba/Ca, and detrital elements (e.g. Al/Ca) showed weaker annual expression. In contrast, the longer periodicities (~1.6 mm and ~4 mm) were clearly expressed in Sr/Ca, Ba/Ca, and detrital proxies, indicating multiannual variability.

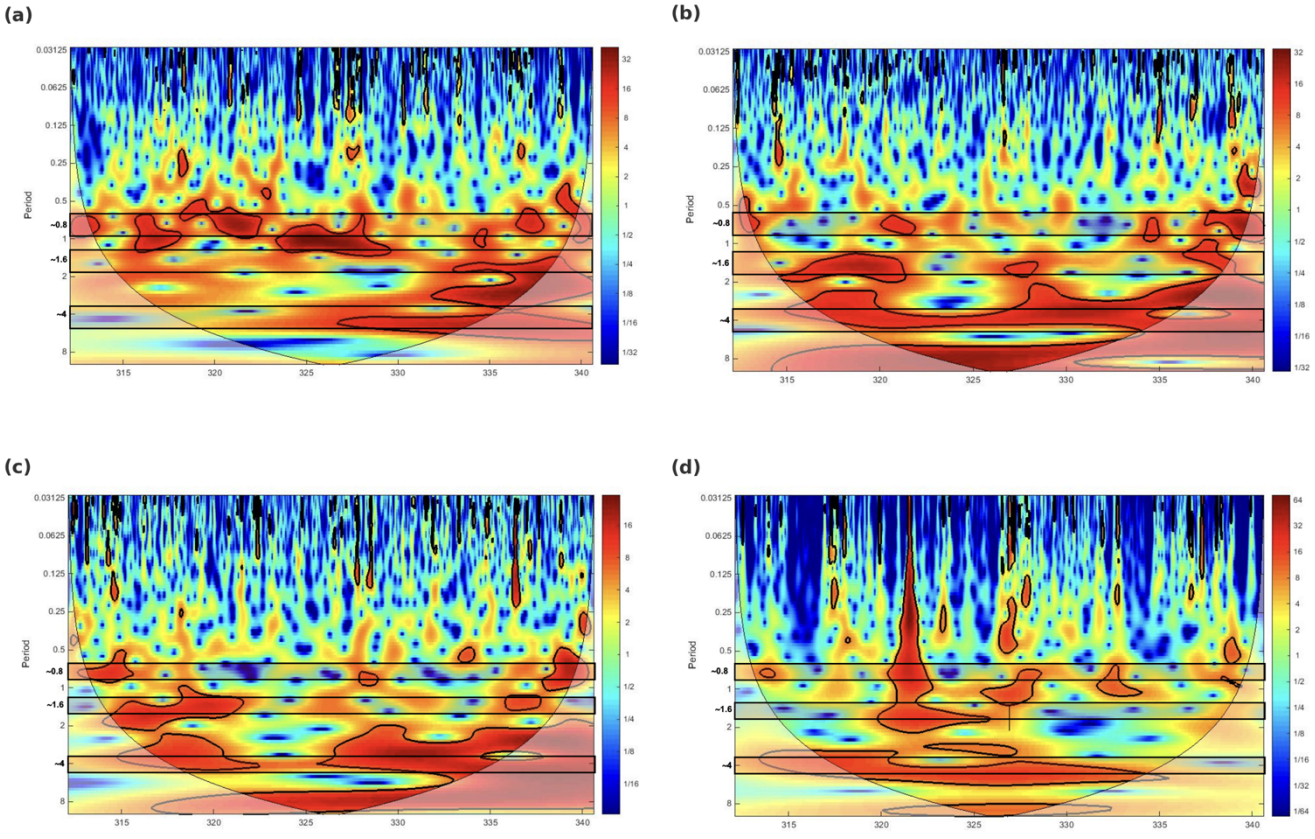

Figure 6. The figure presents the periodicity of Mg/Ca (a), Sr/Ca (b), Ba/Ca (c) and Al/Ca (d) concentrations measured by LA-ICP-MS in the high-resolution dataset of the basal zone of the Zerolín speleothem, using the continuous wavelet transform. The x-axis represents the distance from the top of the speleothem, and the y-axis shows the period in millimetres. Warmer colors indicate higher periodicity power, whereas cooler colors indicate lower power. The warm-colored areas enclosed by a black contour correspond to regions where the detected periodicity is significant at the 95% confidence level. Black rectangles highlight the sectors with the most relevant periodicity.

https://doi.org/10.5194/egusphere-2026-3717
Preprint. Discussion started: 7 July 2026

Wavelet coherence analyses between elemental records indicated scale-dependent relationships: for instance, Mg/Ca and Sr/Ca exhibited an inverse phase relationship at the annual scale and a direct relationship at multiyear scales (Fig. A4, Appendix A). The high spatial resolution of the LA-ICP-MS profiles allows identification of short-wavelength variability across multiple trace elements. In contrast, solution analyses provide smoother trends that emphasize the signal of ions incorporated into the carbonate matrix. Both datasets reveal significant intra-layer variability along the 20 mm transect.

4.6 Speleothem as a paleoclimate proxy

Color analysis along the growth axis of the Zerolín speleothem revealed a systematic alternation of bright and dark laminae, which closely follow visible layering in the basal laminated section. Dark laminae are visually dense and compact, whereas bright layers appear porous and irregular.

The differences between the two types of layers, at the statistical level, showed that dark layers are significantly enriched in Sr ($F_{2,104} = 19.97$; $p < 0.001$; $\eta^2 = 0.277$), Ba ($F_{2,104} = 14.985$; $p < 0.001$; $\eta^2 = 0.224$), and $\delta^{13}C$ ($F_{2,104} = 5.992$; $p = 0.03$; $\eta^2 = 0.103$), while bright laminae exhibit significantly higher concentrations of P ($F_{2,104} = 9.733$; $p < 0.001$; $\eta^2 = 0.158$) and Y ($F_{2,104} = 9.733$; $p < 0.001$; $\eta^2 = 0.158$). The Mg content shows a general trend toward higher levels in the bright, porous calcite layers, and lower levels in the dense, dark ones. These variations are also reflected in the red index of color, which was used to characterize color transitions (Fig. 4).

Trace element ratios and isotope data plotted against the laminae reveal that brightness minima tend to correspond to peaks in Sr/Ca, Ba/Ca and $\delta^{13}C$ values, while brighter sections co-occur with increases in P and Y content. $\delta^{18}O$ values exhibit minor but consistent fluctuations that track the lamination pattern, although no statistically significant differences were found between bright and dark layers for this isotope in the ANOVA ($p > 0.05$).

These geochemical and colorimetric patterns are further illustrated in Fig. 4, which shows the annual variations in color, trace elements and stable isotopes across the basal laminated section. The observed cyclicity in the geochemical signatures suggests a strong seasonal control on lamina formation.

5 Discussion

5.1 Geochemical processes and controls on trace-element ratios variability

Some trace-element ratios act as sensitive proxies of hydroclimatic variability and water–rock interactions within the epikarst, integrating the effects of degassing and PCP, prolonged interaction with dolomite and silicate-rich soils, and episodic detrital inputs. This combination generates characteristic trace-element/Ca patterns that record variability from seasonal to interannual scales. Among them, Mg/Ca exhibits the highest amplitude variations, with relative enrichments during intervals consistent with reduced effective recharge (Fig. 7). This pattern is consistent with observations from other dolomitic karst systems, where dolomite dissolution, residence-time effects, and degassing and PCP are key drivers of Mg enrichment (Fairchild & Treble,

https://doi.org/10.5194/egusphere-2026-3717
Preprint. Discussion started: 7 July 2026

2009; Johnson et al., 2006; Tremaine & Froelich, 2013; Wong et al., 2011; Zhou et al., 2011). The monitoring of modern dripwater in Ardales Cave (Table A1, Appendix A) confirms this behaviour: in April 2016, under exceptionally dry conditions documented by AEMET (22 mm of monthly precipitation; ~50 % of the average monthly precipitation), Mg/Ca ratios were 17 times higher than in the very humid event of March 2018. This striking enrichment was accompanied by longer drip intervals (~20 minutes), consistent with matrix-flow infiltration and prolonged interaction with dolomite and silicate-rich soils, whereas in the wet period (drip interval ~50 s) fissure flow dominated, suppressing Mg enrichment (Belli et al., 2017; Rutlidge et al., 2014; Thoma et al., 1992; Tremaine & Froelich, 2013; Zimmerman et al., 1993).

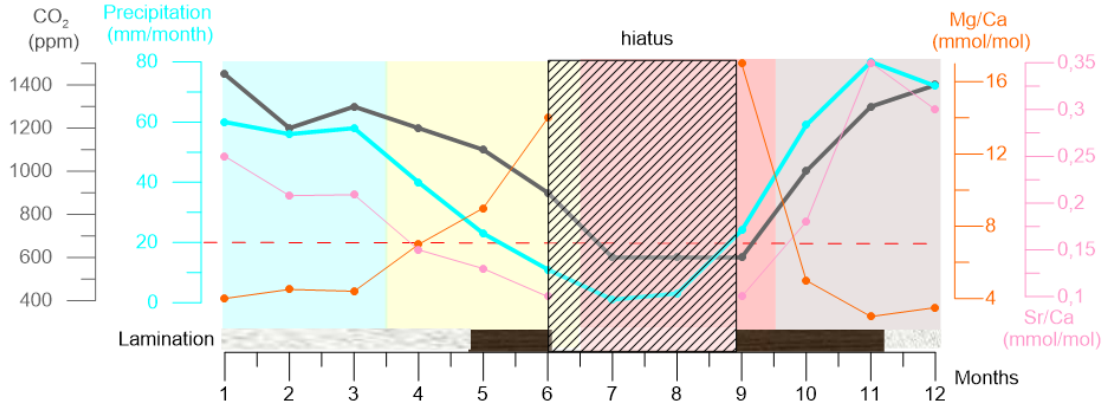

Figure 7. Conceptual model illustrating annual climatic processes in Ardales, showing monthly precipitation (blue line) and cave ventilation intensity (grey line), and their relationship with trace-element ratios in the speleothem: Mg/Ca (orange line) and Sr/Ca (pink line). The blue line represents mean monthly precipitation based on instrumental records from the Campillos station (AEMET, 1899–present), while cave CO_2 levels and ventilation intensity are derived from measurements reported by Fernández-Cortés et al. (2022). The four seasons are indicated by colored background bands: winter (blue), spring (yellow), summer (red), and autumn (brown). Periods of low precipitation (monthly values < 20 mm, marked with a red dashed line) are associated with potential depositional hiatuses, as inferred from I-STAL modeling based on recent dripwater monitoring. The Mg/Ca ratio peaks during dry seasons, influenced by reduced effective recharge, prolonged water residence times in silicate-rich soils and dolomitic host rock, and, where saturation conditions allow, degassing and PCP. In contrast, Sr/Ca reaches its maximum during wet seasons, associated with higher calcite growth rates. The timing of porous light-colored laminae and dense dark laminae is also indicated: the latter are linked to major autumn rainfall events, whereas the former are mainly deposited during the non-ventilated winter period.

In contrast, Sr/Ca and Ba/Ca show a more subdued response, reflecting their stronger dependence on calcite growth rate and associated partition coefficients, together with soil-leaching inputs (Fairchild et al., 2001; Fairchild & Treble, 2009; Stoll et al., 2012). The direct Sr–Ba and inverse Sr–Mg correlations observed here mirror trends described in other Mediterranean

https://doi.org/10.5194/egusphere-2026-3717
Preprint. Discussion started: 7 July 2026

caves (Belli et al., 2017; Huang et al., 2001). Differences in calcite microstructure and porosity may further modulate these signals, consistent with textural variability expected under changing supersaturation (Boch et al., 2011; Muñoz-García et al., 2012).

Consistent with the results, the relationship between Mg/Ca and Al/Ca reflects a detrital component influencing the Mg signal (Riechelmann et al., 2023), as indicated by the significant positive Mg–Al correlation, a relationship also observed in speleothems from sites with episodic soil-erosion inputs. At the same time, the residence time in silicate-rich soils above the cave can increase Mg/Ca and Ba/Ca relative to Sr/Ca (Rutlidge et al., 2014), reinforcing that multiple processes contribute to Mg/Ca and Ba/Ca variability beyond the coupled degassing-and-PCP pathway alone.

The first principal component (PC1) captures the balance between colloidal/detrital phases and carbonate-bound signals, with positive loadings for colloid-associated elements in the LA-ICP-MS dataset (Fig. 5) and negative loadings for P and Y in the solution dataset (Fig. A3, Appendix A) (Fairchild & Treble, 2009; Riechelmann et al., 2020). This pattern reflects the complementary selectivity of the two analytical approaches: LA-ICP-MS, which is sensitive to colloidal and organic-complexed trace metals incorporated into speleothems and solution-based ICP-MS in weak acid, which yields a homogenized signal of the bulk carbonate composition after dissolution (Hartland et al., 2014; Jochum et al., 2012). This analytical context explains why the same underlying processes can project differently across datasets while describing a coherent hydrogeochemical framework.

Sulphur (S/Ca) shows a positive correlation with P/Ca, As/Ca, and Y/Ca, while its relationship with Mg/Ca is negative (Table 1). The study by Wynn et al. (2018) on sulphate associated with carbonate in speleothems showed that pH is the dominant variable controlling the abundance of sulphate in calcite. Thus, a higher pH increases the efficiency of sulphate incorporation into calcite. This efficiency is further enhanced when the stalagmite growth rate is high. Even if the initial aqueous sulphate concentration is low, its incorporation into calcite will be greater if the degree of impurities on the calcite crystal surface is high. Such impurities are associated with higher calcite supersaturation in the dripwater or with high growth rates. Another conclusion reached by the same study is that PCP has no effect on S in stalagmites, since the environmental drivers that mainly regulate its incorporation are ventilation and temperature. P and Y are often associated with the presence of colloids and are therefore usually interpreted as increasing during infiltration events capable of transporting them (Fairchild & Treble, 2009; Huang et al., 2001). The significant correlation between these elements and S may indicate that, in areas where the ratios of all three increase in calcite, the dripwater flow was high, the growth rate was elevated, and/or the droplets were more supersaturated. Therefore, their maxima should correspond to periods of abundant rainfall, when the cave is ventilated and CO_2 levels decrease, or when the growth rate was higher.

Finally, I-STAL modelling of dripwater (Stoll et al., 2012) confirms that at drip intervals longer than ~15 minutes, $CaCO_3$ precipitation becomes negligible (Fig. A1, Appendix A). This implies that the exceptionally dry 2016 event, with ~20-minute drip intervals, would not have contributed calcite to the stalagmite, thereby generating potential depositional hiatuses. The model also shows that Mg/Ca values above ~6 mmol/mol require additional processes beyond degassing and PCP, consistent with contributions from dolomite and silicate-rich soils observed in the modern dripwater. In this context, aridity may reduce

https://doi.org/10.5194/egusphere-2026-3717
Preprint. Discussion started: 7 July 2026

soil pCO_2 and lower the initial saturation state of dripwater, thereby limiting the potential for degassing and PCP even when drip rates decrease (Stoll et al., 2023; Perez-Mejias et al., 2025).

Overall, the integrated evidence supports a process model in which degassing and PCP, residence time over dolomite, detrital/colloidal inputs, soil pCO_2-controlled initial saturation state, and growth-rate changes jointly structure the trace-element record, with PC2 capturing the coupled degassing-and-PCP, growth-rate, and residence-time controls triad and PC1 reflecting the detrital/colloidal axis.

5.2 Stable isotope signals and their decoupling from trace elements ratios

At the scale resolved by trench sampling, $\delta^{13}C$ and $\delta^{18}O$ show a weak but significant positive correlation ($r \approx 0.29$), whereas neither isotope exhibits robust correlations with Mg/Ca (Table 1). This pattern suggests that degassing and PCP cannot be the sole control on the isotopic composition, and that distinct environmental and in-cave processes govern $\delta^{13}C$ and $\delta^{18}O$, respectively (cf. Chiarini et al., 2017; Lachniet, 2009). Hendy tests could not be performed due to the extreme thinness of individual laminae toward the flanks of the growth axis, so kinetic effects cannot be entirely excluded; however, the internal consistency of the proxies supports a scenario in which $\delta^{13}C$ responds to the initial soil–epikarst carbon component and to subsequent modification by coupled degassing and PCP, whereas $\delta^{18}O$ reflects climatic controls on moisture source, amount, and temperature.

This interpretation is consistent with the absence of a strong relationship between $\delta^{13}C$ and Mg/Ca. If $\delta^{13}C$ enrichment were mainly driven by coupled CO_2 degassing and PCP, a clearer response in PCP-sensitive proxies would generally be expected. The absence of such a relationship therefore points to a mixed $\delta^{13}C$ signal, combining an initial soil–epikarst carbon component with a variable overprint by coupled degassing and PCP (Stoll et al., 2023). Under drier conditions, reduced soil respiration and lower soil pCO_2 may shift the initial soil–epikarst carbon component toward higher $\delta^{13}C$ values. However, lower soil pCO_2 can also reduce the initial saturation state of dripwater and therefore its potential for PCP (Stoll et al., 2023). This reduction in PCP potential may explain why some dry intervals do not show a clear PCP-related Mg/Ca increase, but it should not be interpreted as a mechanism producing PCP-related $\delta^{13}C$ enrichment independently of Mg/Ca. Instead, the partial decoupling between $\delta^{13}C$ and Mg/Ca is more plausibly explained by the nonlinear dependence of PCP on drip interval and initial saturation state, superimposed on a variable initial soil–epikarst carbon signal (Stoll et al., 2023). In the present record, this interpretation is further supported by the trace-element framework, which indicates that Mg/Ca does not scale exclusively with coupled degassing and PCP. Where cave ventilation and seasonal microclimate promote CO_2 loss and dripwaters remain sufficiently supersaturated, this pathway may still contribute to $\delta^{13}C$ enrichment and to Mg/Ca variability, but the measured Mg/Ca response is not expected to be strictly proportional to the isotopic enrichment (Mattey et al., 2010; Stoll et al., 2023). $\delta^{18}O$ integrates atmospheric fractionation history and seasonal moisture-source variability (e.g., synoptic winter systems vs. summer convection), with temperature playing a secondary role (Bar-Matthews et al., 1999; Hendy, 1971; Lachniet, 2009; Mattey et al., 2010; Polag et al., 2010). Accordingly, a strict one-to-one seasonal imprint on $\delta^{18}O$ is not expected, and short-scale compensation among amount, source, and temperature can limit any systematic contrast at the lamina scale.

https://doi.org/10.5194/egusphere-2026-3717
Preprint. Discussion started: 7 July 2026

Trace-element ratios behaviour further clarifies this partial decoupling. Ba/Ca exhibits a positive association with $\delta^{13}C$ ($r \approx 0.27$), consistent with growth-rate effects and degassing and PCP operating under hydrogeochemical states that also elevate $\delta^{13}C$, while Mg/Ca does not show a robust seasonal-scale correlation with either isotope due to its mixed sensitivity to degassing and PCP, residence time over dolomite, initial saturation state, and detrital/colloidal inputs (Chiarini et al., 2017; JOHNSON et al., 2006; D. P. Mattey et al., 2010; Treble et al., 2003; Vansteenberge et al., 2020). These relationships align with the PCA structure: PC2 encapsulates coupled degassing-and-PCP, growth-rate, and residence-time controls that influence $\delta^{13}C$ and Ba/Ca similarly, whereas PC1 contrasts colloid/detrital contributions against carbonate-bound signals without imposing a direct isotopic signature

Taken together, the isotope–traces ensemble indicates a system where $\delta^{13}C$ reflects the soil–vegetation carbon component of the dripwater, modulated by soil pCO_2 variability and variably overprinted by cave ventilation and degassing and PCP, while $\delta^{18}O$ records climatic variability in moisture source/amount/temperature, and trace elements register the concurrent action of degassing and PCP, residence-time, and colloidal/detrital inputs. This multi-proxy, multi-process view explains the weak $\delta^{13}C$–$\delta^{18}O$ coupling, the lack of strong isotope–Mg linkages, and the selective $\delta^{13}C$–Ba affinity through growth-rate partitioning.

5.3 Seasonal lamina formation and the role of cave ventilation

The laminated section of the Zerolín stalagmite shows a clear alternation between dark compact laminae and light porous laminae (Fig. 4), whose geochemical signatures have been statistically evaluated through ANOVA tests. The variance analysis revealed that Sr/Ca ($p < 0.001$), Ba/Ca ($p < 0.001$), and $\delta^{13}C$ ($p = 0.03$) values are higher in the dark compact laminae, whereas the porous light laminae are characterized by higher ratios of P/Ca ($p < 0.001$) and Y/Ca ($p < 0.001$).

These results are consistent with previous observations from laminated speleothems formed under Mediterranean climates (Chiarini et al., 2017). In our record, the light porous laminae, with irregular surfaces and higher incorporation of foreign particles and colloids, show lower Sr/Ca concentrations and are associated with irregular drip rates and slower growth. The negative correlation between Sr/Ca and Mg/Ca further suggests marginally drier conditions during the formation of porous laminae. In contrast, the dark compact laminae, with higher Sr/Ca and Ba/Ca contents and lower Mg/Ca, indicate faster growth and wetter conditions, followed by relatively dry periods and then major autumn infiltration events (Fig. 7).

The $\delta^{13}C$ signal also shows systematic differences between lamina types. Higher $\delta^{13}C$ values in the compact laminae are interpreted as reflecting a more positive initial soil–epikarst carbon component during phases of reduced soil respiration and/or lower soil pCO_2. A possible additional overprint by coupled degassing and PCP may also have contributed where dripwater remained sufficiently supersaturated, particularly during intervals of enhanced cave ventilation, in line with the enhanced summer ventilation at Ardales Cave, and in agreement with the modern analogue from St. Michaels Cave in Gibraltar (Mattey et al., 2010). During spring to autumn (April–November) enhanced cave ventilation promotes CO_2 loss, raises pH, and enhances the coupled degassing-and-PCP pathway when dripwater remained sufficiently supersaturated. Compact calcite formation therefore likely reflects ventilated phases and/or the reactivation of dripwater supply after dry intervals, once sufficient supersaturation was restored. Conversely, during winter (November–April), reduced ventilation results in higher

https://doi.org/10.5194/egusphere-2026-3717
Preprint. Discussion started: 7 July 2026

cave air pCO_2, weaker coupled degassing and PCP, and more negative $\delta^{13}C$ values, favouring the precipitation of porous calcite with open intracrystalline pores filled with water.

The $\delta^{18}O$ signal is influenced by seasonal differences in rainfall sources. Winter precipitation, isotopically lighter, reaches the speleothem attenuated due to mixing and storage in the epikarst, whereas summer storms, isotopically heavier, can be further enriched during enhanced cave ventilation and degassing (Mattey et al., 2008). This seasonal isotopic behavior is comparable to the processes described for our site and may also be modulated at multidecadal timescales by winter temperature variations. Taken together, these results suggest that the dark compact laminae formed during spring–summer–autumn (April–November), coinciding with cave ventilation and/or during recharge pulses following summer drought, when dripwater supply resumed under conditions still favourable for calcite supersaturation, which in this site leads to dense fabrics due to the rapid precipitation from a thin water film under supply-limited conditions. Conversely, the light porous laminae formed mainly during the less ventilated winter season (November–April), when higher cave air pCO_2 reduced coupled degassing and PCP and thicker water films favored the incorporation of colloids and intracrystalline voids (Dreybrodt, 1999; Fairchild & Baker, 2012; D. Mattey et al., 2008). Major autumn rainfall events are recorded as the onset of new compact laminae, whereas prolonged summer droughts with monthly precipitation below ~20 mm likely produced short depositional hiatuses, as also supported by I-STAL modeling of modern dripwater conditions (Fig. 7).

Table 2 summarizes the seasonal and environmental interpretation of the lamina types in the Zerolín speleothem.

Lamina type, texture, geochemical signal	Season (inferred)	Ventilation	Soil pCO_2 / initial saturation state	Degassing and PCP
 **Dark, compact** Dense calcite High $\delta^{13}C$, $\delta^{18}O$, Sr y Ba Low Mg	Late spring to early autumn (April-November)	High	Potentially lower soil pCO_2 during dry phases; supersaturation may increase during recharge pulses	Moderate to high
Bright, porous Greater incorporation of foreign ions/colloids into its structure (e.g., P, Y...) Low $\delta^{13}C$, $\delta^{18}O$ y Ba High Mg	Late autumn to early spring (November-April)	Low	Relatively higher soil influence and/or lower effective supersaturation	Low to moderate

Table 2. Summary of seasonal and environmental interpretation of lamina types in the Zerolín speleothem. Own elaboration

5.4 Annual to multiannual periodicities linked to hydroclimatic mode

Wavelet analysis of the basal laminated section of Zerolín reveals robust periodicities at approximately 0.8 mm, 1.6 mm, and 4 mm (Fig. 6), which correspond to annual and multiannual cycles when calibrated against the estimated growth rate (~800 µm/year). The ~0.8 mm periodicity, clearly expressed in Mg/Ca concentrations, supports the interpretation of annual layering

https://doi.org/10.5194/egusphere-2026-3717
Preprint. Discussion started: 7 July 2026

and reinforces the accuracy of the constructed age model for this section. Also, confirming the annual nature of the laminae and validating the use of color-based age interpolation supports by Bayesian model and wingeol lamination tool.

In contrast, multiannual periodicities (~2 and ~5 years) were more prominent in Sr/Ca, Ba/Ca, and detrital element concentrations (e.g. Al/Ca), suggesting responses to interannual hydroclimatic variability. The coherence wavelet analysis (Fig. A4, Appendix A) showed that these proxies exhibit scale-dependent relationships—particularly between Mg/Ca and Sr/Ca—pointing to distinct underlying processes. At the annual scale, Mg/Ca and Sr/Ca showed inverse phasing, while their multiannual variability was more synchronized.

These patterns are consistent with the operation of climate-driven mechanisms such as varying infiltration dynamics and degassing and PCP, which modulate Mg/Ca and Sr/Ca incorporation into speleothem calcite. The enhanced signal in detrital elements at multiyear scales further suggests episodic mobilization linked to shifts in precipitation intensity and frequency. Such variability aligns with known expressions of the NAO in the western Mediterranean, where ~2-5-year oscillations in precipitation have been documented (e.g., Andreo et al., 2006; Rodrigo et al., 1999, 2000; Rust et al., 2022). While external forcings like solar cycles may influence regional climate over longer timescales, the periodicities detected in Zerolín in this section predominantly reflect annual- and multiannual hydroclimatic dynamics.

5.5 Climate variability reconstructed for Southern Iberia during the end of Medieval Climate Anomaly and the Little Ice Age.

The Zerolín stalagmite from Ardales Cave (Málaga) is located in a hydroclimatically sensitive transition zone influenced by both Atlantic and Mediterranean regimes. Building on the site context and modern monitoring presented above, we interpret Mg/Ca variations in Zerolín primarily as a proxy for changes in effective recharge and epikarst residence time, mediated by prolonged water–rock interaction with dolomitic marbles and, where the initial saturation state allows, by degassing and PCP during intervals of reduced infiltration (Fairchild et al., 2001; Sinclair et al., 2012; Treble et al., 2003). In southern Iberia, such conditions are typically intensified during the prolonged late spring–summer–early autumn dry season, when infiltration is limited and epikarst residence time increases (Martin et al., 2014; Cohuet et al., 2011; Gonzalez-Hidalgo et al., 2024; Ruiz-Sinoga et al., 2012; Vicente-Serrano et al., 2004).

Accordingly, higher Mg/Ca ratios reflect sustained or intensified dry conditions and stronger residence-time and dolomitic imprint, with possible contribution from degassing and PCP, whereas lower Mg/Ca ratios indicate more effective recharge and higher drip rates. During the driest intervals, reduced calcite precipitation may generate short depositional hiatuses, an effect further evaluated using I-STAL model simulations (Stoll et al., 2012). Finally, while intense Mediterranean rainfall events associated with cut-off lows (DANAs) may episodically reactivate infiltration after droughts, the Mg/Ca signal is interpreted here as integrating the preceding dry-phase geochemical imprint rather than representing a direct seasonal rainfall signal (Halifa-Marin et al., 2021; Perez & García, 2023; Martinez-Artigas et al., 2021; Miró et al., 2022).

Following this reasoning and focusing on the Mg/Ca concentration as the primary hydroclimate proxy, complemented by the growth rate and $\delta^{13}C$ records, four distinct periods of significant environmental dry conditions are evident. These intervals are

https://doi.org/10.5194/egusphere-2026-3717
Preprint. Discussion started: 7 July 2026

characterized by high or very high Mg/Ca concentrations, relative to the long-term mean which is considered the climatological baseline for the studied interval.

These periods of elevated Mg/Ca are robustly supported by opposite trends in the other proxies. They coincide precisely with minima in the speleothem's growth rate and are accompanied by higher $\delta^{13}C$ values. This multi-proxy combination with high Mg/Ca (indicating aridity-related residence-time and hydrogeochemical conditions), low growth rate (consistent with reduced recharge), and higher $\delta^{13}C$ (compatible with a more positive initial soil–epikarst carbon component, with possible overprinting by coupled degassing and PCP where dripwater remained sufficiently supersaturated) , allows these intervals to be defined as significantly dry, or as periods of pronounced hydroclimatic aridity. The first and most prominent of these events occurs at the termination of the Medieval Climate Anomaly, centered at approximately 1125 AD, where Mg/Ca ratios reach their maximum for the entire record. Three subsequent arid events are identified around 1250 AD, shortly before 1500 AD, and the second most significant event, which occurs at approximately 1560 AD (Fig. 8).

https://doi.org/10.5194/egusphere-2026-3717
Preprint. Discussion started: 7 July 2026

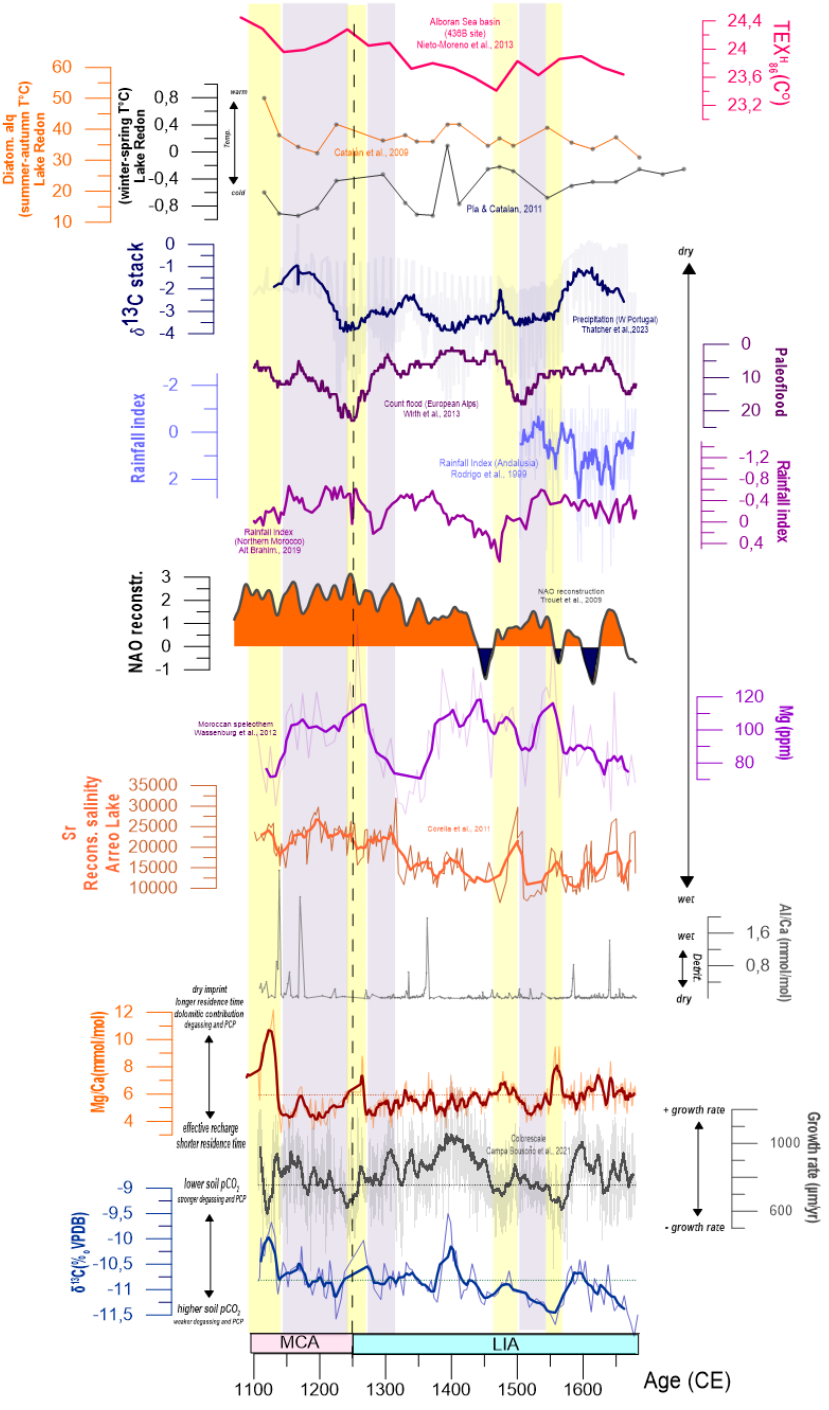

Figure 8. From top to bottom: (1) Alboran Sea basin temperature reconstruction (dark pink; Nieto-Moreno et al., 2013); (2) summer–autumn temperature reconstruction from Lake Redon (orange; Catalán et al., 2009); winter–spring temperature reconstruction from Lake Redon (black; Plá & Catalán, 2011); (3) reconstructed precipitation in Portugal based on $\delta^{13}C$ (blue;

https://doi.org/10.5194/egusphere-2026-3717
Preprint. Discussion started: 7 July 2026

Thatcher et al., 2023) (4) palaeoflood frequency in the Central Alps (maroon; Wirth et al., 2013); (5) precipitation index in Andalusia (light blue; Rodrigo et al., 1999); (6) rainfall index in northern Morocco (dark purple; Ait Brahim et al., 2019); (7) reconstructed NAO index (black; Trouet et al., 2009); (7) Mg-based speleothem aridity reconstruction in Morocco (purple; Wassenburg et al., 2012); (8) Sr-based salinity reconstruction from Lake Arreo (Corella et al., 2011); record digitized from the figure presented in Morellón et al. (2012) due to the unavailability of the original dataset. Lower panels correspond to the Zerolín speleothem data from this study: (9) Al/Ca ratio (grey) with running average (dark grey); (10) Mg/Ca ratio (orange) with running average (dark orange); (11) growth rate derived from colour quantification (grey; following Campa-Bousoño et al., 2021); (12) $\delta^{13}C$ (blue) with running average (dark blue). Yellow boxes indicate Mg peaks associated with extreme aridity events, whereas puple boxes mark the most humid periods. White boxes indicate periods in which there has been a proliferation of autumn precipitation events associated with cut-off lows (DANAS), resulting in high hydroclimatological variability, but always close to the climatological average.

In opposition to these arid phases, the record reveals corresponding humid intervals. These are most notable between 1150 and 1200 AD, around 1300 AD, and at 1520 AD. During these periods, Mg/Ca concentrations are significantly lower than the long-term mean and are concurrently associated with high growth rates and more negative $\delta^{13}C$ values, a proxy assemblage collectively suggesting sustained humid conditions (Fig. 8).

However, two significant climatic intervals within the study period exhibit a geochemical behavior that deviates from the criteria established above: the period between approximately 1320 AD and 1450 AD, and the interval from 1600 AD to 1700 AD (Fig. 8).

As observed in Fig. 8, the geochemical signature during these phases is not as uniform as in the clearly defined arid and humid periods. Instead, the Mg/Ca record shows much higher variability, oscillating closer to the proxy's long-term mean, although with notable excursions above it. Critically, these periods are characterized by high, or very high, growth rates (particularly the 1320–1450 AD interval) and $\delta^{13}C$ values that are not as high as those seen during the pronounced arid events.

It is here that the influence of significant autumnal precipitation of Mediterranean origin, associated with the presence of DANAs (cut-off lows), becomes a key explanatory factor. We propose these are periods where, although arid conditions (in the sense of sustained drought) are not dominant, the precipitation regime has shifted. These Mediterranean events are typically torrential and highly localized in time (Llasat et al., 2016, 2021; Machado et al., 2011), capable of delivering large accumulations that restore hydroclimatic conditions toward the climatological norm or even above normal if these events are connected with post plentiful winter precipitation, thus driving the observed high growth rates.

However, these events climatologically occur at the end of the summer dry period, which likely coincides with the end of a seasonal depositional hiatus. The system is therefore already primed by the preceding summer drought, which has elevated the Mg/Ca ratios in the epikarst reservoir. Consequently, the ensuing torrential (end of summer-autumn) precipitation flushes this high-Mg/Ca solution into the speleothem system. This mechanism results in elevated Mg/Ca signals being recorded, despite the abundant precipitation that simultaneously fosters an increase in the growth rate.

https://doi.org/10.5194/egusphere-2026-3717
Preprint. Discussion started: 7 July 2026

We therefore interpret these intervals not merely as climatologically neutral—that is, neither fully arid nor fully humid—but rather as periods reflecting a significant shift in the dominant mode of general atmospheric circulation. This shift manifests as a greater influence of Mediterranean-sourced precipitation, associated with synoptic patterns conducive to the formation of cut-off lows (or DANAs). This typically involves an Atlantic configuration dominated by subtropical high pressure in the vicinity of the Iberian Peninsula, which effectively blocks Atlantic frontal systems (Martin et al., 2014; Ulbrich et al., 2012; Hidalgo-Muñoz et al., 2011). This blocking is concurrent, however, with a powerful, meandering jet stream. This meandering fosters the isolation of polar air masses at low latitudes (Sousa et al., 2016, 2017; Scherrer et al., 2006). This setup, combined with the significant moisture advection and sharp thermal contrast provided by the warm Mediterranean Sea, creates an ideal "breeding ground" for the proliferation of these instability events, which generate abundant, torrential precipitation in the late summer and autumn. This represents a classic atmospheric configuration known to be associated with the dynamics of cold periods, such as the Little Ice Age, which is precisely the timeframe in which these two distinct episodes occur.

It is critical to contextualize this record by noting the significant scarcity of high-resolution paleoclimatic archives spanning this period specifically within the southern Iberian region of Andalusia. While regional reconstructions exist, such as those presented in Figure 8, they are often situated in areas where the climatological signal is more decisively dominated by either a purely Atlantic regime (Portugal or the Atlantic coast of Morocco)(Santos et al., 2024; Mora &Vieira, 2020; Hakam et al., 2025) or by Mediterranean and convective regimes (Pyrenees or the interior peninsula) (Gallart et al., 2002; Gonzalez-Hidalgo et al., 2024). Therefore, the Zerolín record constitutes an unprecedented archive from a critical transitional area, offering a unique opportunity to investigate the hydroclimatic history of a region sensitive to both Atlantic and Mediterranean forcings.

Despite its regional complexity, the distinct hydroclimatic phases identified within the Zerolín speleothem record (representing arid and humid excursions from the climatological mean) are not isolated local phenomena. On the contrary, they demonstrate a remarkably robust coherence with both regional-scale hydroclimatic proxies and hemispheric-scale atmospheric circulation patterns documented across the Western Mediterranean (Fig. 8). The primary driver for this variability appears to be the North Atlantic Oscillation (NAO). A visual inspection reveals a strikingly strong positive correspondence between the Zerolín Mg/Ca record and the NAO reconstruction. Each of the four principal arid phases (high Mg/Ca) aligns precisely with one of the four most significant positive NAO peaks in the reconstruction (Trouet et al., 2009). This relationship is mechanistically sound, as persistent positive NAO phases (NAO+) are known to strengthen the Azores High, effectively blocking the penetration of Atlantic storm tracks into Iberia and inducing widespread arid conditions (Trigo et al., 2002, 2004; García-Herrera et al., 2007; Vicente-Serrano, 2006).

This NAO-driven interpretation is unequivocally validated by the synchronous response of other independent regional proxies. The aridity record from the Moroccan speleothem (Wassenburg et al., 2012), for instance, exhibits a near-identical pattern to the Zerolín Mg/Ca, confirming that these arid events were large-scale, synchronous episodes affecting both southern Iberia and northwestern Africa. This signal is further corroborated by the Arreo Lake salinity reconstruction (Corella et al., 2011), a separate paleolimnological archive, where the high Mg/Ca (arid) phases in Zerolín match intervals of high lacustrine salinity (a classic indicator of a negative precipitation-evaporation balance). Furthermore, these signals are inversely mirrored in

https://doi.org/10.5194/egusphere-2026-3717
Preprint. Discussion started: 7 July 2026

precipitation-based reconstructions: the high Mg/Ca excursions align also with periods of reduced precipitation documented in the rainfall indices for Andalusia and Northern Morocco, as well as with drier conditions inferred from the $\delta^{13}C$ stack from Portugal (Ait Brahim; 2019; Rodrigo et al., 1999; Thatcher et al., 2023). Taken together, the Zerolín Mg/Ca proxy serves as a high-fidelity recorder of the regional hydroclimatic expression of NAO-driven atmospheric variability during the MCA–LIA transition.

In the two periods where Mediterranean precipitation regime appears to dominate (1320–1450 AD and 1600–1700 AD), the relationship with the broader array of regional proxies from Figure 8 is no longer clear, exhibiting notable variability and decoupling, directly connected with periods where there are significant transitions between different NAO conditions. During these intervals, the Zerolín record does not correlate strongly with the aridity signals from the Moroccan speleothem or the Arreo Lake salinity, nor does it consistently track the rainfall indices from Portugal or Andalusia. This decoupling is, in itself, diagnostically significant. What we propose is that this lack of regional coherence is a direct consequence of the governing atmospheric mechanism. While the formation of DANAs (cut-off lows) requires the presence of well-defined, large-scale synoptic ingredients (such as a potent subtropical anticyclone accompanied by a strong, meandering jet stream) their hydroclimatic consequences are often markedly localized.

Modern climatological studies focusing specifically on severe rainfall in the southern Spanish provinces, including the Ardales study area, confirm that such events are frequently caused by cut-off lows isolated from the main flow (Halifa-Marin et al., 2021; Perez & García, 2023; Martinez-Artigas et al., 2021; Miró et al., 2022). These studies demonstrate that different atmospheric clusters can produce entirely different meteo-climatic outcomes over distances of less than 500 km, supporting the observed proxy divergence from sites in Portugal, Morocco, or the Pyrenees (Santos et al., 2024; Mora &Vieira, 2020; Hakam et al., 2025; Gallart et al., 2002; Gonzalez-Hidalgo et al., 2024, Martin et al., 2014; Ulbrich et al., 2012; Hidalgo-Muñoz et al., 2011). This mechanism allows for hydroclimatically significant precipitation to occur under both positive or negative mean NAO states, depending entirely on the specific characteristics and positioning of the cut-off low. This highlights the critical value of the Zerolín record in differentiating between periods dominated by homogenous, large-scale Atlantic forcing (i.e., NAO-driven) and these distinct intervals where localized, convective Mediterranean dynamics played a more significant role in modulating the regional hydroclimate.

6 Conclusions

This study provides an exceptionally high-resolution and regionally rare multiproxy record of hydroclimatic variability from the Zerolín stalagmite in Ardales Cave (southern Iberia), covering a climatically unstable interval between the late MCA and the early LIA. The integration of U/Th dating, lamina counting, and color index analysis has yielded a robust and internally consistent chronology, enabling sub-annual to annual interpretations of environmental variability during this key climatic transition.

https://doi.org/10.5194/egusphere-2026-3717
Preprint. Discussion started: 7 July 2026

The alternation between compact and porous laminae, together with variations in trace-element ratios and stable isotopes, reflects marked seasonal and interannual changes in moisture availability, infiltration dynamics, and cave ventilation. Mg/Ca emerges as a sensitive proxy for drought conditions, mainly controlled by epikarst residence time,dolomitic water–rock interaction, initial saturation state, and the coupled effects of degassing and PCP rather than by direct rainfall amount. Meanwhile, Sr/Ca and Ba/Ca ratios capture signals related to growth rate, recharge intensity, and soil contributions, while the isotopic composition provides complementary information on soil pCO_2, initial dissolved inorganic carbon, effective infiltration, moisture sources, and subsequent degassing and PCP. Taken together, this multiproxy consistency highlights the capacity of the Zerolín record to trace both seasonal-scale processes and longer hydroclimatic oscillations in this Mediterranean karst system. Moreover, the interpretation of these proxies is reinforced by the strong internal coherence among independent indicators and by model-based assessments of karst hydrology, ensuring a robust climatic signal despite potential kinetic effects.

From a paleoclimatic perspective, the Zerolín record captures alternating humid and arid phases across the MCA–LIA transition. Four main dry intervals, centered at approximately 1125, 1250, 1500, and 1560 AD, correspond to elevated Mg/Ca ratios, reduced growth rates, and enriched $\delta^{13}C$ values, indicative of prolonged droughts and reduced infiltration. In contrast, wetter phases around 1150–1200, 1300, and 1520 AD show the opposite signal combination. Furthermore, two additional episodes (1320–1450 and 1600–1700 AD) display complex behaviour, likely reflecting enhanced Mediterranean convective precipitation (DANAs) during periods of weakened Atlantic influence.

In addition, the detection of multiannual periodicities (~2–5 years) in trace-element variability supports a possible connection with atmospheric circulation modes such as the North Atlantic Oscillation (NAO), which strongly influence precipitation in the western Mediterranean. The timing of the main arid phases coincides with positive NAO modes, when a strengthened Azores High limits the penetration of Atlantic storm tracks, promoting aridity across Iberia. Conversely, intervals dominated by Mediterranean convective systems coincide with transitional NAO conditions, emphasizing the dual climatic control—Atlantic versus Mediterranean—that governs southern Iberian hydroclimate.

Although the Zerolín record is robust, some methodological limitations should be considered. The establishment of the chronological framework was constrained by the moderate uranium concentration of the speleothem, its porosity, and its relatively young age (ca. 1000 years), which together limited the precision of U/Th dating. Additionally, the geochemical characterization of the feeding dripwater was performed using different analytical techniques, reducing direct comparability among measurements. Finally, the Hendy test was not carried out, so isotopic equilibrium for $\delta^{18}O$ and $\delta^{13}C$ could not be confirmed or ruled out.

Nevertheless, by integrating geochemical proxies, petrographic observations, internal consistency analyses, and forward modelling, this study demonstrates the effectiveness of a combined methodological approach for disentangling seasonal to multiannual hydroclimatic variability in Mediterranean karst systems. The Zerolín speleothem thus represents a key archive from a transitional climatic zone, where both Atlantic westerlies and Mediterranean convective systems leave a distinct imprint

https://doi.org/10.5194/egusphere-2026-3717
Preprint. Discussion started: 7 July 2026

on recharge and speleothem growth. Importantly, the resolution achieved in this record enables a detailed characterization of the MCA–LIA transition, revealing sequences of short-term fluctuations embedded within longer-term hydroclimatic shifts. Overall, this study refines the understanding of hydroclimatic variability in southern Iberia, showing that droughts and pluvials during the last millennium were shaped by alternating dominance of Atlantic (NAO+) and Mediterranean (DANA-type) modes. The Zerolín record illustrates how high-resolution speleothems can bridge local karst processes with regional and hemispheric circulation dynamics, providing a valuable framework for future paleoclimate reconstructions in the western Mediterranean.

Appendix A

1 Modern dripwater geochemistry

1.1 Methods

Drip water samples were analyzed for major cations and anions using high-performance ion chromatography (Metrohm 881 IC Pro), and alkalinity was determined via automatic titration (Metrohm 888 Titrando) (Barberá et al., 2018). Another set of drip water samples was analyzed using an ICP-MS-QQQ, following the procedure and instrument specifications described in the Methods section of the main article.

1.2 Results

Dripwater samples were collected during two contrasting hydrological periods: April 2016, characterized as dry, and March 2018, classified as very wet, based on AEMET meteorological data (Table A1). The geochemical composition of the dripwater showed marked differences between both events. Mg/Ca ratios were 17 times higher during the dry period compared to the very wet period. Sr/Ca and Ba/Ca ratios also increased during the dry period, by factors of approximately 4.8 and 6.4, respectively (Table A1).

Date	Monthly precipitation (mm)	% of average monthly precipitation	Pluviometric character	Mg/Ca (mmol/mol)	Sr/Ca (mmol/mol)	Ba/Ca (mmol/mol)
April 2016	22.0	50%	Dry	1466.02	3.78	0.134
March 2018	193.4	375%	Very wet	86.10	0.78	0.021

Table A1. Precipitation data are based on monthly records from the Spanish Meteorological Agency (AEMET). Geochemical values refer to the composition of dripwater collected inside Ardales Cave during contrasting hydrological conditions. Ratios are expressed in mmol/mol and elemental concentrations in parts per million (ppm).

https://doi.org/10.5194/egusphere-2026-3717
Preprint. Discussion started: 7 July 2026

Elemental concentrations measured in the dripwater confirm these trends, with Mg concentrations of 25.08 ppm in 2016 vs. 7.05 ppm in 2018, Sr values of 0.25 ppm vs. 0.23 ppm, and Ba values of 0.013 ppm vs. 0.0097 ppm. Ca concentrations were notably lower during the dry period (28.22 ppm) compared to the wet period (135.1 ppm). Drip rate measurements at the sampling location indicated a drop interval of ~20 minutes in April 2016, and ~50 seconds in March 2018.

Modeling with I-STAL using these measured drip intervals, two initial Ca concentrations (30 and 120 ppm), and fixed cave parameters (17 °C, 900 ppm CO_2), showed that drip intervals longer than ~15 minutes resulted in negligible $CaCO_3$ deposition under both modeled scenarios (Fig. A1). The geochemical analysis of Zerolín revealed a wide variation in Mg/Ca ratios. While PCP is likely the dominant process influencing Mg/Ca variations, its effect is limited to a range set by the host rock composition and the $CaCO_3$ solubility threshold (Stoll et al., 2012). I-STAL simulations indicate that Mg/Ca values above ~6 mmol/mol cannot be explained by PCP alone, suggesting the involvement of additional processes.

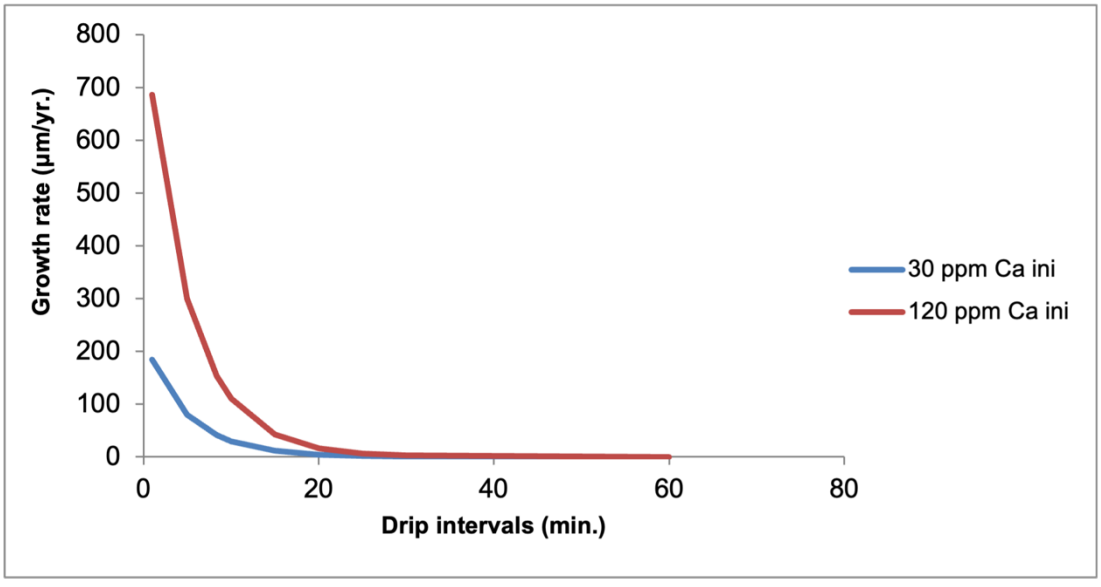

Figure A1. Growth rate of the Zerolín stalagmite estimated from I-STAL simulations based on drip interval. The model incorporates $CaCO_3$ degassing and precipitation dynamics to infer calcite accumulation under varying hydrological conditions.

To assess how these modern values compare with those recorded in the stalagmite, we calculated the Mg/Ca and Sr/Ca ratios of the inferred dripwater based on the measured trace-element concentrations in annual sectors of the Zerolín speleothem (Figure A2), using several published partition coefficients (e.g. Day & Henderson, 2013; Fairchild et al., 2010; Gascoyne, 1983; Tremaine & Froelich, 2013). Dripwater Mg/Ca and Sr/Ca, inferred from stalagmite Mg/Ca and Sr/Ca in the basal laminated section, ranged from 112-1154 mmol/mol and 0.54-2.39 mmol/mol, respectively, using partition coefficients DMg (Day & Henderson, 2013) and DSr (Tremaine & Froelich, 2013).

https://doi.org/10.5194/egusphere-2026-3717
Preprint. Discussion started: 7 July 2026

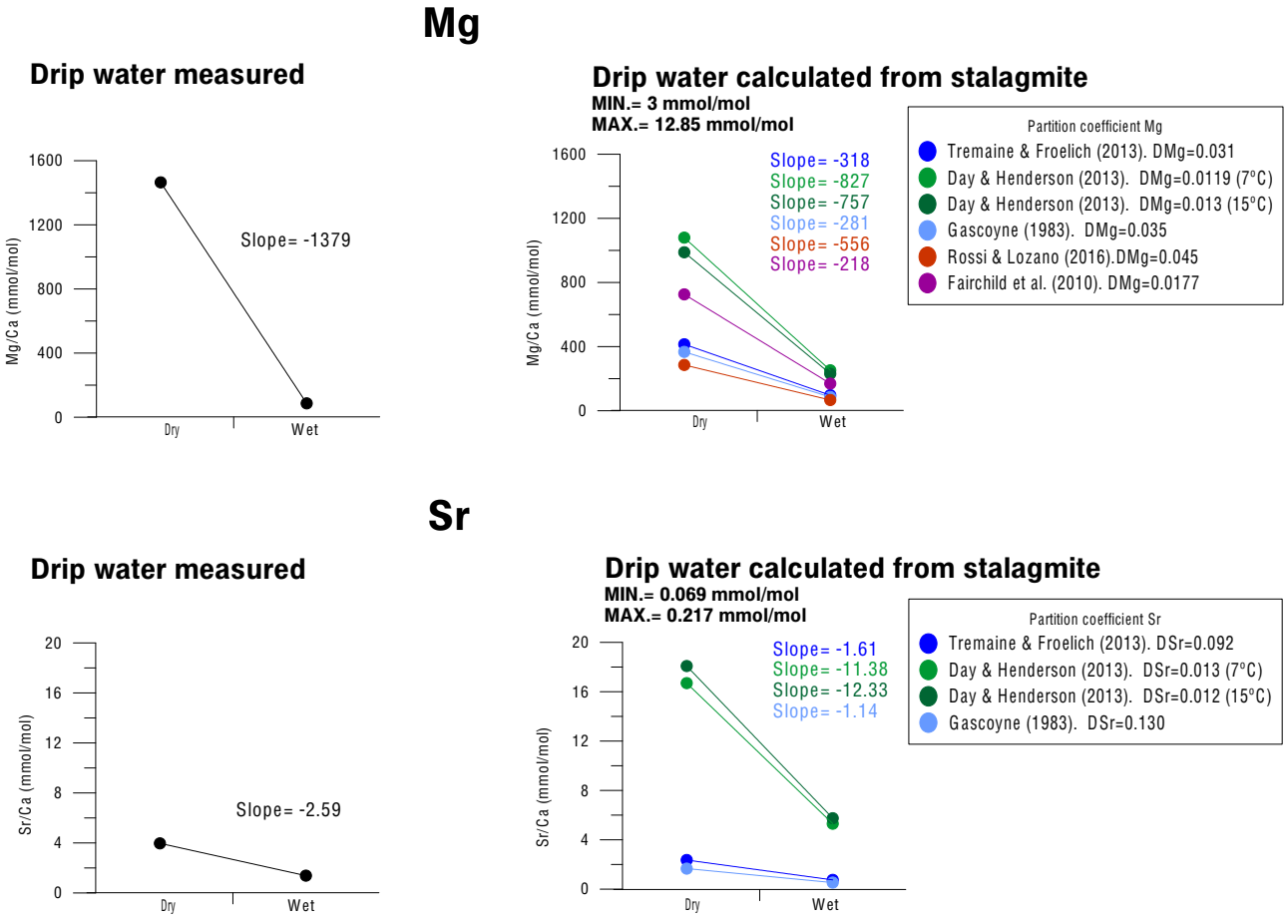

Figure A2. Comparison between Mg/Ca and Sr/Ca ratios measured in modern drip water and those calculated from the Zerolín stalagmite (Mg/Castalagmite: max/min = 12.85/3 mmol/mol; Sr/Castalagmite: max/min = 0.217/0.069 mmol/mol). Partition coefficients were adjusted according to values proposed by different authors in order to reconcile the trace-element concentrations in stalagmite-derived drip water with modern observations.

The measured modern dripwater ratios in 2016 and 2018 lie outside the range of values inferred from the speleothem in anual sector, indicating that the geochemical extremes observed in recent years were not reached during the analyzed portion of the annual record.

https://doi.org/10.5194/egusphere-2026-3717
Preprint. Discussion started: 7 July 2026

2 Figures

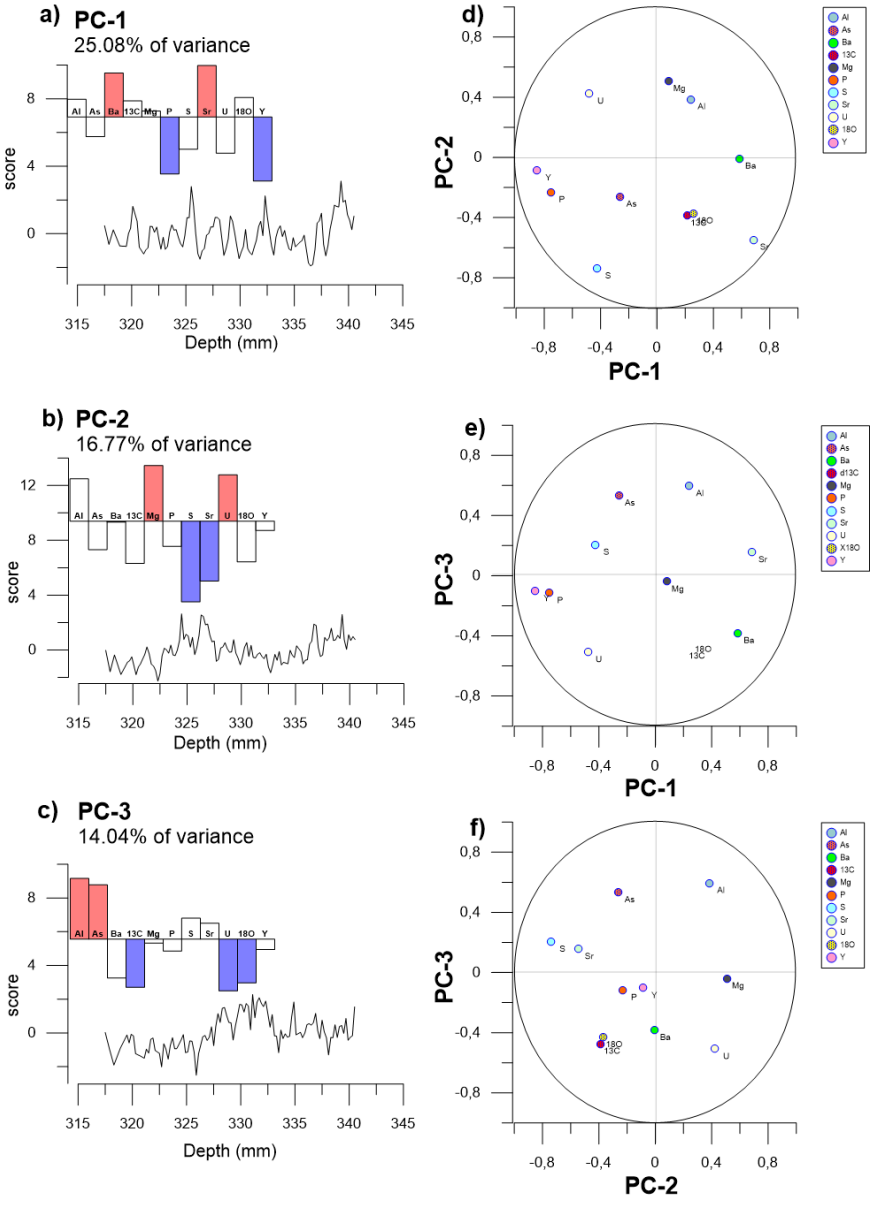

Figure A3. Principal component analysis (PCA) of 11 variables including nine trace element concentrations measured by solution-based ICP-MS-QQQ (27Al, 75As, 138Ba, 25Mg, 31P, 32S, 86Sr, 238U, 89Y) and two stable isotope ratios ($\delta^{13}C$ and $\delta^{18}O$). Panels A-C show PCA scores for PC1 to PC3 plotted against distance in the annually laminated section of the speleothem. The percentage of total variance explained by each component is indicated in each panel. Panels D-F display

https://doi.org/10.5194/egusphere-2026-3717
Preprint. Discussion started: 7 July 2026

variable loadings for PC2 vs. PC1, PC3 vs. PC1, and PC3 vs. PC2. Loadings are color-coded (red = positive association, blue = negative association). The unit circle defines the maximum loading range.

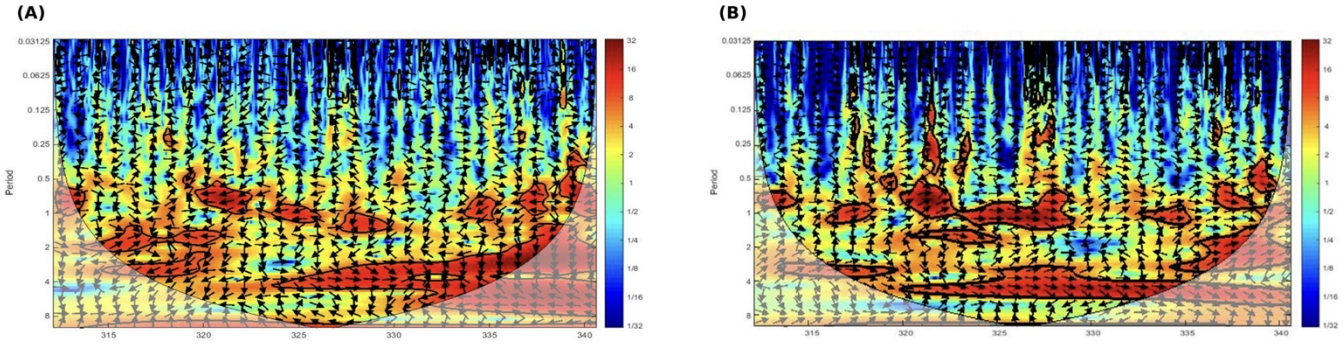

Figure A4. The figure shows the wavelet coherence analysis of the high-resolution geochemical record from the lower section of the Zerolín speleothem, based on trace-element concentrations measured by LA-ICP-MS. Arrows indicate the phase relationship between the paired series: rightward arrows denote in-phase relationships, whereas leftward arrows denote anti-phase relationships. The panels display the coherence between Mg/Ca and Sr/Ca ratios (A), and between Mg/Ca and Al/Ca concentrations (B).

3 Tables

	Mg	Al	Cu	Zn	Sr	Y	Ba	Pb
Mg	1	**0.349****	0.226**	**0.430****	-0.121**	0.114**	0.112**	**0.301****
Al		1	0.159**	**0.343****	-0.024	0.210**	0.130**	**0.259****
Cu			1	**0.479****	0.045*	0.090**	0.102**	0.175**
Zn				1	0.082**	0.181**	0.248**	**0.402****
Sr					1	-0.032	**0.566****	0.267**
Y						1	0.135**	0.236**
Ba							1	**0.436****
Pb								1

Table A2. Pearson correlation coefficients among trace elements analyzed using LA-ICP-MS. Values marked with * are significant at $p < .05$; those marked with ** are significant at $p < .01$. Values highger than +-.25 are highglihted in bold for easy identification.

https://doi.org/10.5194/egusphere-2026-3717
Preprint. Discussion started: 7 July 2026

Code and data availability

The Zerolín speleothem data presented in this study are currently subject to an embargo by the University of Oviedo until November 2030 and therefore cannot be made publicly available at this stage. Until the embargo expires, data access requests may be addressed to the corresponding author and will be evaluated in accordance with applicable university policies. After the embargo period, the dataset is intended to be submitted for inclusion in a subsequent version of the SISAL database.

Supplement link

The link to the supplement will be included by Copernicus, if applicable.

Author contributions

CC and HS conceived and designed the study. CC conducted the measurements, curated and analysed the data, and wrote the first draft of the manuscript. MI performed the U–Th chronology, with support from HC and RLE. JP provided laboratory facilities and guidance for the acquisition, use, and interpretation of the LA-ICP-MS data. IV and LO coordinated and supported the fieldwork in Málaga. HS, MI, IV, and JP provided scientific supervision and methodological guidance throughout the study. All authors contributed to the interpretation and discussion of the results, critically revised the manuscript, and approved the final version for publication.

Competing interests

The contact author has declared that none of the authors has any competing interests.

Disclaimer

Copernicus Publications remains neutral with regard to jurisdictional claims made in the text, published maps, institutional affiliations, or any other geographical representation in this paper. While Copernicus Publications makes every effort to include appropriate place names, the final responsibility lies with the authors. Views expressed in the text are those of the authors and do not necessarily reflect the views of the publisher.

Acknowledgements

Celia Campa and Heather Stoll acknowledge financial support from the Agencia Estatal de Investigación (Ministerio de Ciencia e Innovación, Spain) and Universidad de Oviedo. The authors are grateful to Ana Méndez from the Grupo de Espectroscopia, Láseres y Plasmas (GELP) for laboratory assistance. The authors also thank Pedro Cantalejo, Director of

https://doi.org/10.5194/egusphere-2026-3717
Preprint. Discussion started: 7 July 2026

Ardales Cave, for his continuous support and collaboration, particularly in facilitating access to the cave and the collection of the speleothem record. Finally, the authors thank the anonymous reviewers for their valuable comments and constructive suggestions, which significantly improved the quality of this manuscript.

Financial support

This research was supported by the Agencia Estatal de Investigación (Ministerio de Ciencia e Innovación, Spain) through project OPERA (CTM2013-48639-C2-1-R). Additional funding was provided by Universidad de Oviedo through project UNOV-16-RLD-UE-3.

Review statement

The review statement will be added by Copernicus Publications listing the handling editor as well as all contributing referees according to their status anonymous or identified.

References

Ait Brahim, Y., Wassenburg, J. A., Sha, L., Cruz, F. W., Deininger, M., Sifeddine, A., ... and Cheng, H.: North Atlantic ice-rafting, ocean and atmospheric circulation during the Holocene: Insights from Western Mediterranean speleothems, Geophys. Res. Lett., 46, 7614–7623, https://doi.org/10.1029/2019GL082405, 2019.

Andreo, B., Jiménez, P., Durán, J. J., Carrasco, F., Vadillo, I., and Mangin, A.: Climatic and hydrological variations during the last 117–166 years in the south of the Iberian Peninsula, from spectral and correlation analyses and continuous wavelet analyses, J. Hydrol., 324, 24–39, https://doi.org/10.1016/j.jhydrol.2005.09.010, 2006.

Baker, A., Smith, C., Jex, C., Fairchild, I., Genty, D., and Fuller, L.: Annually laminated speleothems: a review, Int. J. Speleol., 37, 193–206, 2008.

Bar-Matthews, M., Ayalon, A., Kaufman, A., and Wasserburg, G. J.: The Eastern Mediterranean paleoclimate as a reflection of regional events: Soreq Cave, Israel, Earth Planet. Sci. Lett., 166, 85–95, https://doi.org/10.1016/S0012-821X(98)00275-1, 1999.

Barberá, J. A., Jódar, J., Custodio, E., González-Ramón, A., Jiménez-Gavilán, P., Vadillo, I., Pedrera, A., and Martos-Rosillo, S.: Groundwater dynamics in a hydrologically-modified alpine watershed from an ancient managed recharge system (Sierra Nevada National Park, Southern Spain): Insights from hydrogeochemical and isotopic information, Sci. Total Environ., 640–641, 874–893, https://doi.org/10.1016/j.scitotenv.2018.05.305, 2018

https://doi.org/10.5194/egusphere-2026-3717
Preprint. Discussion started: 7 July 2026

Bartolomé, M., Moreno, A., Sancho, C., Cacho, I., Stoll, H., Haghipour, N., Belmonte, Á., Spötl, C., Hellstrom, J., Edwards, R. L., and Cheng, H.: Reconstructing hydroclimate changes over the past 2500 years using speleothems from Pyrenean caves (NE Spain), Clim. Past, 20, 467–494, https://doi.org/10.5194/cp-20-467-2024, 2024.

Belli, R., Borsato, A., Frisia, S., Drysdale, R., Maas, R., and Greig, A.: Investigating the hydrological significance of stalagmite geochemistry (Mg, Sr) using Sr isotope and particulate element records across the Late Glacial-to-Holocene transition, Geochim. Cosmochim. Acta, 199, 247–263, https://doi.org/10.1016/j.gca.2016.10.024, 2017.

Bini, M., Zanchetta, G., Regattieri, E., Isola, I., Drysdale, R. N., Fabiani, F., Genovesi, S., and Hellstrom, J. C.: Hydrological changes during the Roman Climatic Optimum in northern Tuscany (Central Italy) as evidenced by speleothem records and archaeological data, J. Quat. Sci., 35, 791–802, https://doi.org/10.1002/jqs.3224, 2020.

Beguería, S., Peña-Angulo, D., Trullenque-Blanco, V., and González-Hidalgo, C.: MOPREDAScentury: a long-term monthly precipitation grid for the Spanish mainland, Earth Syst. Sci. Data, 15, 2547–2575, https://doi.org/10.5194/essd-15-2547-2023, 2023.

Blyth, A. J., Asrat, A., Baker, A., Gulliver, P., Leng, M. J., and Genty, D.: A new approach to detecting vegetation and land-use change using high-resolution lipid biomarker records in stalagmites, Quat. Res., 68, 314–324, https://doi.org/10.1016/j.yqres.2007.08.002, 2007.

Boch, R., Spötl, C., and Frisia, S.: Origin and palaeoenvironmental significance of lamination in stalagmites from Katerloch Cave, Austria, Sedimentology, 58, 508–531, https://doi.org/10.1111/j.1365-3091.2010.01173.x, 2011.

Breitenbach, S. F. M. and Bernasconi, S. M.: Carbon and oxygen isotope analysis of small carbonate samples (20 to 100 µg) with a GasBench II preparation device, Rapid Commun. Mass Spectrom., 25, 1910–1914, https://doi.org/10.1002/rcm.5052, 2011.

Campa-Bousoño, C., García-Pérez, Á., Moreno, A., Iglesias, M., Cheng, H., Edwards, R. L., and Stoll, H.: Continuous color model as a tool to improve speleothem age model development, Int. J. Speleol., 50, 313–326, https://doi.org/10.5038/1827-806X.50.3.2389, 2021.

Cantalejo, P.: Cueva de Ardales (Málaga, España). Patrimonio Prehistórico en el Sur de la Península Ibérica, in: Pleistocene foragers on the Iberian Peninsula: Their culture and environment, edited by: Pastoors, A. and Auffermann, B., Neanderthal Museum, 7, 101–117, 2013.

Catalan, J., Pla, S., García, J., and Camarero, L.: Climate and CO_2 saturation in an alpine lake throughout the Holocene, Limnol. Oceanogr., 54, 2542–2552, https://doi.org/10.4319/lo.2009.54.6_part_2.2542, 2009.

Chiarini, V., Couchoud, I., Drysdale, R., Bajo, P., Milanolo, S., Frisia, S., Greig, A., Hellstrom, J., and De Waele, J.: Petrographical and geochemical changes in Bosnian stalagmites and their palaeo-environmental significance, Int. J. Speleol., 46, 33–49, https://doi.org/10.5038/1827-806X.46.1.2057, 2017.

Cisneros, M., Cacho, I., Frigola, J., Moreno, A., Stoll, H., Fornós, J. J., Sigró, J., and Barriendos, M.: Exploring a Mallorca cave flooding during the Little Ice Age using nondestructive techniques on a stalagmite: micro-CT and XRF core scanning, Quat. Res., 118, 75–87, https://doi.org/10.1017/qua.2023.52, 2024.

https://doi.org/10.5194/egusphere-2026-3717
Preprint. Discussion started: 7 July 2026

Cohuet, J. B., Romero, R., Homar, V., Ducrocq, V., and Ramis, C.: Initiation of a severe thunderstorm over the Mediterranean Sea, Atmos. Res., 100, 603–620, https://doi.org/10.1016/j.atmosres.2010.11.002, 2011.

Corella Aznar, J. P.: Climate and human impact in northern Spain since Mid-Holocene: The high resolution records of Lakes Arreo and Montcortès, Ph.D. thesis, University of Zaragoza, Spain, 2011.

Day, C. C. and Henderson, G. M.: Controls on trace-element partitioning in cave-analogue calcite, Geochim. Cosmochim. Acta, 120, 612–627, https://doi.org/10.1016/j.gca.2013.05.044, 2013.

de Villiers, S., Greaves, M., and Elderfield, H.: An intensity ratio calibration method for the accurate determination of Mg/Ca and Sr/Ca of marine carbonates by ICP-AES, Geochem. Geophys. Geosyst., 3, https://doi.org/10.1029/2001GC000169, 2002.

Dreybrodt, W.: Chemical kinetics, speleothem growth and climate, Boreas, 28, 347–356, https://doi.org/10.1111/j.1502-3885.1999.tb00224.x, 1999.

Fairchild, I. J. and Baker, A.: Speleothem Science: From Process to Past Environments, John Wiley & Sons, Chichester, United Kingdom, ISBN 9781405196208, 2012.

Fairchild, I. J., Baker, A., Borsato, A., Frisia, S., Hinton, R. W., McDermott, F., and Tooth, A. F.: Annual to sub-annual resolution of multiple trace-element trends in speleothems, J. Geol. Soc., 158, 831–841, https://doi.org/10.1144/jgs.158.5.831, 2001.

Fairchild, I. J., Spötl, C., Frisia, S., Borsato, A., Susini, J., Wynn, P. M., and Cauzid, J.: Petrology and geochemistry of annually laminated stalagmites from an Alpine cave (Obir, Austria): seasonal cave physiology, Geol. Soc. Lond. Spec. Publ., 336, 295–321, https://doi.org/10.1144/SP336.16, 2010.

Fairchild, I. J. and Treble, P. C.: Trace elements in speleothems as recorders of environmental change, Quaternary Sci. Rev., 28, 449–468, https://doi.org/10.1016/j.quascirev.2008.11.007, 2009.

Fernandez-Cortes, A., Martin-Pozas, T., Cuezva, S., Cañaveras, J. C., Saiz-Jimenez, C., and Sanchez-Moral, S.: Unraveling the drivers controlling the transient and seasonal CO_2 dynamic in a shallow temperate cave, Geosciences, 12, 335, https://doi.org/10.3390/geosciences12090335, 2022.

Frisia, S.: Microstratigraphic logging of calcite fabrics in speleothems as tool for palaeoclimate studies, Int. J. Speleol., 44, 1–16, http://dx.doi.org/10.5038/1827-806X.44.1.1, 2015.

Frisia, S., Borsato, A., Fairchild, I. J., and McDermott, F.: Calcite fabrics, growth mechanisms, and environments of formation in speleothems from the Italian Alps and southwestern Ireland, J. Sediment. Res., 70, 1183–1196, https://doi.org/10.1306/022900701183, 2000.

Frisia, S., Borsato, A., Spötl, C., Villa, I. M., and Cucchi, F.: Climate variability in the SE Alps of Italy over the past 17 000 years reconstructed from a stalagmite record, Boreas, 34, 445–455, https://doi.org/10.1080/03009480500231336, 2005.

Gagnon, J. E., Fryer, B. J., Samson, I. M., and Williams-Jones, A. E.: Quantitative analysis of silicate certified reference materials by LA-ICP-MS with and without an internal standard, J. Anal. At. Spectrom., 23, 1529–1537, https://doi.org/10.1039/B801807N, 2008.

https://doi.org/10.5194/egusphere-2026-3717
Preprint. Discussion started: 7 July 2026

878 Gallart, F., Llorens, P., Latron, J., and Regüés, D.: Hydrological processes and their seasonal controls in a small Mediterranean
879 mountain catchment in the Pyrenees, Hydrol. Earth Syst. Sci., 6, 527–537, https://doi.org/10.5194/hess-6-527-2002, 2002.
880 García-Barrón, L., Morales, J., and Sousa, A.: Characterisation of the intra-annual rainfall and its evolution (1837–2010) in
881 the southwest of the Iberian Peninsula, Theor. Appl. Climatol., 114, 445–457, https://doi.org/10.1007/s00704-013-0855-7,
882 2013.
883 García-Herrera, R., Hernández, E., Barriopedro, D., Paredes, D., Trigo, R. M., Trigo, I. F., and Mendes, M. A.: The outstanding
884 2004/05 drought in the Iberian Peninsula: associated atmospheric circulation, J. Hydrometeorol., 8, 483–498,
885 https://doi.org/10.1175/JHM578.1, 2007.
886 Gascoyne, M.: Trace-element partition coefficients in the calcite-water system and their paleoclimatic significance in cave
887 studies, J. Hydrol., 61, 213–222, https://doi.org/10.1016/0022-1694(83)90249-4, 1983.
888 Gonzalez-Hidalgo, J. C., Trullenque-Blanco, V., Beguería, S., and Peña-Angulo, D.: Seasonal precipitation changes in the
889 western Mediterranean Basin: The case of the Spanish mainland, 1916–2015, Int. J. Climatol., 44, 1800–1815,
890 https://doi.org/10.1002/joc.8412, 2024.
891 Grinsted, A., Moore, J. C., and Jevrejeva, S.: Application of the cross wavelet transform and wavelet coherence to geophysical
892 time series, Nonlin. Processes Geophys., 11, 561–566, https://doi.org/10.5194/npg-11-561-2004, 2004.
893 Hakam, O., Bouras, E. H., Amazirh, A., Ongoma, V., Eddamiri, S., Saidi, L., ... and Chehbouni, A.: Influence of atmospheric
894 and oceanic circulation patterns on precipitation variability in North Africa with a focus on Morocco, Sci. Rep., 15, 17977,
895 https://doi.org/10.1038/s41598-025-02718-0, 2025.
896 Halifa-Marin, A., Lorente-Plazas, R., Pravia-Sarabia, E., Montavez, J. P., and Jimenez-Guerrero, P.: Atlantic and
897 Mediterranean influence promoting an abrupt change in winter precipitation over the southern Iberian Peninsula, Atmos. Res.,
898 253, 105485, https://doi.org/10.1016/j.atmosres.2021.105485, 2021.
899 Hartland, A., Fairchild, I. J., Müller, W., and Dominguez-Villar, D.: Preservation of NOM-metal complexes in a modern
900 hyperalkaline stalagmite: Implications for speleothem trace element geochemistry, Geochim. Cosmochim. Acta, 128, 29–43,
901 https://doi.org/10.1016/j.gca.2013.12.005, 2014.
902 Haslett, J. and Parnell, A.: A simple monotone process with application to radiocarbon-dated depth chronologies, J. R. Stat.
903 Soc. C Appl. Stat., 57, 399–418, https://doi.org/10.1111/j.1467-9876.2008.00623.x, 2008.
904 Hendy, C. H.: The isotopic geochemistry of speleothems—I. The calculation of the effects of different modes of formation on
905 the isotopic composition of speleothems and their applicability as palaeoclimatic indicators, Geochim. Cosmochim. Acta, 35,
906 801–824, https://doi.org/10.1016/0016-7037(71)90127-X, 1971.
907 Hidalgo-Muñoz, J. M., Argüeso, D., Gámiz-Fortis, S. R., Esteban-Parra, M. J., and Castro-Díez, Y.: Trends of extreme
908 precipitation and associated synoptic patterns over the southern Iberian Peninsula, J. Hydrol., 409, 497–511,
909 https://doi.org/10.1016/j.jhydrol.2011.08.049, 2011.

https://doi.org/10.5194/egusphere-2026-3717
Preprint. Discussion started: 7 July 2026

Huang, Y., Fairchild, I. J., Borsato, A., Frisia, S., Cassidy, N. J., McDermott, F., and Hawkesworth, C. J.: Seasonal variations in Sr, Mg and P in modern speleothems (Grotta di Ernesto, Italy), Chem. Geol., 175, 429–448, https://doi.org/10.1016/S0009-2541(00)00337-5, 2001.

Jochum, K. P., Scholz, D., Stoll, B., Weis, U., Wilson, S. A., Yang, Q., Schwalb, A., Börner, N., Jacob, D. E., and Andreae, M. O.: Accurate trace element analysis of speleothems and biogenic calcium carbonates by LA-ICP-MS, Chem. Geol., 318–319, 31–44, https://doi.org/10.1016/j.chemgeo.2012.05.009, 2012.

Johnson, K., Hu, C., Belshaw, N., and Henderson, G.: Seasonal trace-element and stable-isotope variations in a Chinese speleothem: The potential for high-resolution paleomonsoon reconstruction, Earth Planet. Sci. Lett., 244, 394–407, https://doi.org/10.1016/j.epsl.2006.01.064, 2006.

Krichak, S. O. and Alpert, P.: Signatures of the NAO in the atmospheric circulation during wet winter months over the Mediterranean region, Theor. Appl. Climatol., 82, 27–39, https://doi.org/10.1007/s00704-004-0119-7, 2005.

Lachniet, M. S.: Climatic and environmental controls on speleothem oxygen-isotope values, Quaternary Sci. Rev., 28, 412–432, https://doi.org/10.1016/j.quascirev.2008.10.021, 2009.

Lionello, P., Malanotte-Rizzoli, P., and Boscolo, R. (Eds.): Mediterranean Climate Variability, Elsevier, Amsterdam, The Netherlands, Vol. 4, ISBN 9780444521705, 2006.

Llasat, M. C., Marcos, R., Turco, M., Gilabert, J., and Llasat-Botija, M.: Trends in flash flood events versus convective precipitation in the Mediterranean region: The case of Catalonia, J. Hydrol., 541, 24–37, https://doi.org/10.1016/j.jhydrol.2016.05.040, 2016.

Llasat, M. C., del Moral, A., Cortès, M., and Rigo, T.: Convective precipitation trends in the Spanish Mediterranean region, Atmos. Res., 257, 105581, https://doi.org/10.1016/j.atmosres.2021.105581, 2021.

Luterbacher, J., Dietrich, D., Xoplaki, E., Grosjean, M., and Wanner, H.: European seasonal and annual temperature variability, trends, and extremes since 1500, Science, 303, 1499–1503, https://doi.org/10.1126/science.1093877, 2004.

Machado, M. J., Benito, G., Barriendos, M., and Rodrigo, F. S.: 500 years of rainfall variability and extreme hydrological events in southeastern Spain drylands, J. Arid Environ., 75, 1244–1253, https://doi.org/10.1016/j.jaridenv.2011.02.002, 2011.

Mann, M. E., Zhang, Z., Rutherford, S., Bradley, R. S., Hughes, M. K., Shindell, D., Ammann, C., Faluvegi, G., and Ni, F.: Global signatures and dynamical origins of the Little Ice Age and Medieval Climate Anomaly, Science, 326, 1256–1260, https://doi.org/10.1126/science.1177303, 2009.

Martín, J. R., García, M. M., de Pablo Dávila, F., and Soriano, L. R.: Regimes of intense precipitation in the Spanish Mediterranean area, Atmos. Res., 137, 66–79, https://doi.org/10.1016/j.atmosres.2013.09.010, 2014.

Martín-Chivelet, J., Muñoz-García, M. B., Edwards, R. L., Turrero, M. J., and Ortega, A. I.: Land surface temperature changes in Northern Iberia since 4000 yr BP, based on δ13C of speleothems, Global Planet. Change, 77, 1–12, https://doi.org/10.1016/j.gloplacha.2011.02.002, 2011.

https://doi.org/10.5194/egusphere-2026-3717
Preprint. Discussion started: 7 July 2026

Martín-Puertas, C., Jiménez-Espejo, F., Martínez-Ruiz, F., Nieto-Moreno, V., Rodrigo, M., Mata, M. P., and Valero-Garcés, B. L.: Late Holocene climate variability in the southwestern Mediterranean region: an integrated marine and terrestrial geochemical approach, Clim. Past, 6, 807–816, https://doi.org/10.5194/cp-6-807-2010, 2010.

Martinez-Artigas, J., Lemus-Canovas, M., and Lopez-Bustins, J. A.: Precipitation in peninsular Spain: Influence of teleconnection indices and spatial regionalisation, Int. J. Climatol., 41, 1320–1335, https://doi.org/10.1002/joc.6770, 2021.

Mattey, D., Lowry, D., Duffet, J., Fisher, R., Hodge, E., and Frisia, S.: A 53 year seasonally resolved oxygen and carbon isotope record from a modern Gibraltar speleothem: Reconstructed drip water and relationship to local precipitation, Earth Planet. Sci. Lett., 269, 80–95, https://doi.org/10.1016/j.epsl.2008.01.051, 2008.

Mattey, D. P., Fairchild, I. J., Atkinson, T. C., Latin, J.-P., Ainsworth, M., and Durell, R.: Seasonal microclimate control of calcite fabrics, stable isotopes and trace elements in modern speleothem from St Michaels Cave, Gibraltar, Geol. Soc. Lond. Spec. Publ., 336, 323–344, https://doi.org/10.1144/SP336.17, 2010.

Meyer, M. C., Faber, R., and Spötl, C.: The WinGeol Lamination Tool: new software for rapid, semi-automated analysis of laminated climate archives, Holocene, 16, 753–761, https://doi.org/10.1191/0959683606hl969rr, 2006.

Mickler, P. J., Stern, L. A., and Banner, J. L.: Large kinetic isotope effects in modern speleothems, Geol. Soc. Am. Bull., 118, 65–81, https://doi.org/10.1130/B25698.1, 2006.

Miró, J. J., Lemus-Canovas, M., Serrano-Notivoli, R., Cantos, J. O., Estrela, M. J., Martin-Vide, J., ... and Meseguer-Ruiz, O.: A component-based approximation for trend detection of intense rainfall in the Spanish Mediterranean coast, Weather Clim. Extrem., 38, 100513, https://doi.org/10.1016/j.wace.2022.100513, 2022.

Mora, C. and Vieira, G.: The climate of Portugal, in: Landscapes and Landforms of Portugal, edited by: Vieira, G. and Zêzere, J. L., Springer, Cham, Switzerland, 33–46, https://doi.org/10.1007/978-3-319-03641-0_3, 2020.

Morellón, M., Valero-Garcés, B., González-Sampériz, P., Vegas-Vilarrúbia, T., Rubio, E., Rieradevall, M., Delgado-Huertas, A., Mata, P., Romero, Ó., Engstrom, D. R., López-Vicente, M., Navas, A., and Soto, J.: Climate changes and human activities recorded in the sediments of Lake Estanya (NE Spain) during the Medieval Warm Period and Little Ice Age, J. Paleolimnol., 46, 423–452, https://doi.org/10.1007/s10933-009-9346-3, 2011.

Morellón, M., Pérez-Sanz, A., Corella, J. P., Büntgen, U., Catalán, J., González-Sampériz, P., ... and Valero-Garcés, B.: A multi-proxy perspective on millennium-long climate variability in the Southern Pyrenees, Clim. Past, 8, 683–700, https://doi.org/10.5194/cp-8-683-2012, 2012.

Müller, W., Shelley, M., Miller, P., and Broude, S.: Initial performance metrics of a new custom-designed ArF excimer LA-ICP-MS system coupled to a two-volume laser-ablation cell, J. Anal. At. Spectrom., 24, 209–214, https://doi.org/10.1039/B805995K, 2009.

Muñoz-García, M. B., López-Arce, P., Fernández-Valle, M. E., Martín-Chivelet, J., and Fort, R.: Porosity and hydric behavior of typical calcite microfabrics in stalagmites, Sediment. Geol., 265–266, 72–86, https://doi.org/10.1016/j.sedgeo.2012.03.016, 2012.

https://doi.org/10.5194/egusphere-2026-3717
Preprint. Discussion started: 7 July 2026

Neukom, R., Steiger, N., Gómez-Navarro, J. J., Wang, J., and Werner, J. P.: No evidence for globally coherent warm and cold periods over the preindustrial Common Era, Nature, 571, 550–554, https://doi.org/10.1038/s41586-019-1401-2, 2019.

Neves, M. C.: Links Between Extremes in GRACE TWS and Climate Patterns Across Iberia, Water, 17, 1108, https://doi.org/10.3390/w17081108, 2025.

Nuriel, P., Wotzlaw, J.-F., Ovtcharova, M., Vaks, A., Stremtan, C., Šala, M., Roberts, N. M. W., and Kylander-Clark, A. R. C.: The use of ASH-15 flowstone as a matrix-matched reference material for laser-ablation U–Pb geochronology of calcite, Geochronology, 3, 35–47, https://doi.org/10.5194/gchron-3-35-2021, 2021.

Parnell, A. C., Haslett, J., Allen, J. R. M., Buck, C. E., and Huntley, B.: A flexible approach to assessing synchroneity of past events using Bayesian reconstructions of sedimentation history, Quaternary Sci. Rev., 27, 1872–1885, https://doi.org/10.1016/j.quascirev.2008.07.009, 2008.

Pérez, I. A. and García, M. Á.: Climate change in the Iberian Peninsula by weather types and temperature, Atmos. Res., 284, 106596, https://doi.org/10.1016/j.atmosres.2022.106596, 2023.

Pérez-Mejías, C., Wang, J., Ning, Y., Moreno, A., Delgado-Huertas, A., Edwards, R. L., Cheng, H., and Stoll, H. M.: Climate controls on speleothem initial 234U/238U ratios in midlatitude settings over two glacial cycles, Geochim. Cosmochim. Acta, 389, 265–279, https://doi.org/10.1016/j.gca.2024.11.016 , 2025.

Pla-Rabes, S. and Catalan, J.: Deciphering chrysophyte responses to climate seasonality, J. Paleolimnol., 46, 139–150, https://doi.org/10.1007/s10933-011-9529-6, 2011.

Polag, D., Scholz, D., Mühlinghaus, C., Spötl, C., Schröder-Ritzrau, A., Segl, M., and Mangini, A.: Stable isotope fractionation in speleothems: Laboratory experiments, Chem. Geol., 279, 31–39, https://doi.org/10.1016/j.chemgeo.2010.09.016, 2010.

Ramos, J., Weniger, G. C., Cantalejo, P., and Espejo, M. M.: Cueva de Ardales 2011–2014. Intervenciones Arqueológicas, 2014.

Riechelmann, D. F. C., Jochum, K. P., Richter, D., and Scholz, D.: Mg records of two stalagmites from B7-Cave (northwest Germany) indicating long-term precipitation changes during Early to Mid-Holocene, Int. J. Speleol., 52, 9–22, https://doi.org/10.5038/1827-806X.52.1.2440, 2023.

Riechelmann, D. F. C., Riechelmann, S., Wassenburg, J. A., Fohlmeister, J., Schöne, B. R., Jochum, K. P., Richter, D. K., and Scholz, D.: High-resolution proxy records from two simultaneously grown stalagmites from Zoolithencave (Southeastern Germany) and their potential for palaeoclimate reconstruction, Geochem. Geophys. Geosyst., 21, https://doi.org/10.1029/2019GC008755, 2020.

Rivas-Martínez, S.: Mapa de series de vegetación de España: 1:400 000, Instituto Nacional para la Conservación de la Naturaleza (ICONA), Madrid, Spain, 1987.

Rivas-Martínez, S., Fernández-González, F., Loidi, J., Lousã, M., and Penas, A.: Syntaxonomical checklist of vascular plant communities of Spain and Portugal to association level, Itinera Geobot., 14, 5–341, 2001.

https://doi.org/10.5194/egusphere-2026-3717
Preprint. Discussion started: 7 July 2026

Rodrigo, F. S., Esteban-Parra, M. J., Pozo-Vázquez, D., and Castro-Díez, Y.: A 500-year precipitation record in Southern Spain, Int. J. Climatol., 19, 1233–1253, https://doi.org/10.1002/(SICI)1097-0088(199909)19:11%3C1233::AID-JOC413%3E3.0.CO;2-L, 1999.

Rodrigo, F. S., Esteban-Parra, M. J., Pozo-Vázquez, D., and Castro-Díez, Y.: Rainfall variability in southern Spain on decadal to centennial time scales, Int. J. Climatol., 20, 721–732, https://doi.org/10.1002/1097-0088(20000615)20:7%3C721::AID-JOC520%3E3.0.CO;2-Q, 2000.

Rodrigo-Gámiz, M., García-Alix, A., Jiménez-Moreno, G., Ramos-Román, M. J., Camuera, J., Toney, J. L., Sachse, D., Anderson, R. S., and Sinninghe Damsté, J. S.: Paleoclimate reconstruction of the last 36 kyr based on branched glycerol dialkyl glycerol tetraethers in the Padul palaeolake record (Sierra Nevada, southern Iberian Peninsula), Quaternary Sci. Rev., 281, 107434, https://doi.org/10.1016/j.quascirev.2022.107434, 2022.

Rossi, C. and Lozano, R. P.: Hydrochemical controls on aragonite versus calcite precipitation in cave dripwaters, Geochim. Cosmochim. Acta, 192, 70–96, https://doi.org/10.1016/j.gca.2016.07.021, 2016.

Ruiz-Sinoga, J. D., Garcia-Marin, R., Gabarron-Galeote, M. A., and Martinez-Murillo, J. F.: Analysis of dry periods along a pluviometric gradient in Mediterranean southern Spain, Int. J. Climatol., 32, 1558-1571, https://doi.org/10.1002/joc.2376 , 2012.

Rust, W., Bloomfield, J. P., Cuthbert, M., Corstanje, R., and Holman, I.: The importance of non-stationary multiannual periodicities in the North Atlantic Oscillation index for forecasting water resource drought, Hydrol. Earth Syst. Sci., 26, 2449–2467, https://doi.org/10.5194/hess-26-2449-2022, 2022.

Rutlidge, H., Baker, A., Marjo, C. E., Andersen, M. S., Graham, P. W., Cuthbert, M. O., Rau, G. C., Roshan, H., Markowska, M., Mariethoz, G., and Jex, C. N.: Dripwater organic matter and trace element geochemistry in a semi-arid karst environment: Implications for speleothem paleoclimatology, Geochim. Cosmochim. Acta, 135, 217–230, https://doi.org/10.1016/j.gca.2014.03.036, 2014.

Santos, R. N., Rodrigues, T., Naughton, F., Schefuß, E., Oliveira, D., Moreno, J., ... and Hernández, A.: Understanding the Atlantic influence on climate and vegetation dynamics in western Iberia over the last 2000 years, Quaternary Sci. Rev., 337, 108796, https://doi.org/10.1016/j.quascirev.2024.108796, 2024.

Scherrer, S. C., Croci-Maspoli, M., Schwierz, C., and Appenzeller, C.: Two-dimensional indices of atmospheric blocking and their statistical relationship with winter climate patterns in the Euro-Atlantic region, Int. J. Climatol., 26, 233–249, https://doi.org/10.1002/joc.1250, 2006.

Simmons, A. J.: Trends in the tropospheric general circulation from 1979 to 2022, Weather Clim. Dyn., 3, 777–809, 2022.

Sinclair, D. J., Banner, J. L., Taylor, F. W., Partin, J., Jenson, J., Mylroie, J., Goddard, E., Quinn, T., Jocson, J., and Miklavič, B.: Magnesium and strontium systematics in tropical speleothems from the Western Pacific, Chem. Geol., 294–295, 1–17, https://doi.org/10.1016/j.chemgeo.2011.10.008, 2012.

Stoll, H. M., Müller, W., and Prieto, M.: I-STAL, a model for interpretation of Mg/Ca, Sr/Ca and Ba/Ca variations in speleothems and its forward and inverse application on seasonal to millennial scales, Geochem. Geophys. Geosyst., 13, https://doi.org/10.1029/2012GC004183, 2012.

Stoll, H., Mendez-Vicente, A., Gonzalez-Lemos, S., Moreno, A., Cacho, I., Cheng, H., and Edwards, R. L.: Interpretation of orbital scale variability in mid-latitude speleothem δ18O: Significance of growth rate controlled kinetic fractionation effects, Quaternary Sci. Rev., 127, 215–228, https://doi.org/10.1016/j.quascirev.2015.08.025, 2015.

Stoll, H. M., Day, C., Lechleitner, F., Kost, O., Endres, L., Sliwinski, J., Pérez-Mejías, C., Cheng, H., and Scholz, D.: Distinguishing the combined vegetation and soil component of δ13C variation in speleothem records from subsequent degassing and prior calcite precipitation effects, Clim. Past, 19, 2423–2444, https://doi.org/10.5194/cp-19-2423-2023, 2023.

Sousa, P. M., Barriopedro, D., Trigo, R. M., Ramos, A. M., Nieto, R., Gimeno, L., ... and Liberato, M. L.: Impact of Euro-Atlantic blocking patterns in Iberia precipitation using a novel high resolution dataset, Clim. Dyn., 46, 2573–2591, https://doi.org/10.1007/s00382-015-2718-7, 2016.

Sousa, P. M., Trigo, R. M., Barriopedro, D., Soares, P. M., Ramos, A. M., and Liberato, M. L.: Responses of European precipitation distributions and regimes to different blocking locations, Clim. Dyn., 48, 1141–1160, https://doi.org/10.1007/s00382-016-3132-5, 2017.

Sousa, P. M., Trigo, R. M., Barriopedro, D., Soares, P. M., and Santos, J. A.: European temperature responses to blocking and ridge regional patterns, Clim. Dyn., 50, 457–477, https://doi.org/10.1007/s00382-017-3620-2, 2018.

Suárez-Moreno, R., Kushnir, Y., and Seager, R.: Observational analysis of decadal and long-term hydroclimate drivers in the Mediterranean region: role of the ocean–atmosphere system and anthropogenic forcing, Clim. Dyn., 58, 2079–2107, https://doi.org/10.1007/s00382-021-05765-1, 2022.

Tan, M., Liu, T., Hou, J., Qin, X., Zhang, H., and Li, T.: Cyclic rapid warming on centennial-scale revealed by a 2650-year stalagmite record of warm season temperature, Geophys. Res. Lett., 30, https://doi.org/10.1029/2003GL017352, 2003.

Thatcher, D. L., Wanamaker, A. D., Denniston, R. F., Ummenhofer, C. C., Asmerom, Y., Polyak, V. J., ... and Gillikin, D. P.: Iberian hydroclimate variability and the Azores High during the last 1200 years: evidence from proxy records and climate model simulations, Clim. Dyn., 60, 2365–2387, https://doi.org/10.1007/s00382-022-06427-6, 2023.

Thoma, S. G., Gallegos, D. P., and Smith, D. M.: Impact of fracture coatings on fracture/matrix flow interactions in unsaturated, porous media, Water Resour. Res., 28, 1357–1367, https://doi.org/10.1029/92WR00167, 1992.

Torrence, C. and Compo, G. P.: A practical guide to wavelet analysis, Bull. Am. Meteorol. Soc., 79, 61–78, https://doi.org/10.1175/1520-0477(1998)079%3C0061:APGTWA%3E2.0.CO;2, 1998.

Treble, P., Shelley, J. M. G., and Chappell, J.: Comparison of high resolution sub-annual records of trace elements in a modern (1911–1992) speleothem with instrumental climate data from southwest Australia, Earth Planet. Sci. Lett., 216, 141–153, https://doi.org/10.1016/S0012-821X(03)00504-1, 2003.

Tremaine, D. M. and Froelich, P. N.: Speleothem trace element signatures: A hydrologic geochemical study of modern cave dripwaters and farmed calcite, Geochim. Cosmochim. Acta, 121, 522–545, https://doi.org/10.1016/j.gca.2013.07.026, 2013.

https://doi.org/10.5194/egusphere-2026-3717
Preprint. Discussion started: 7 July 2026

Trigo, R. M., Osborn, T. J., and Corte-Real, J. M.: The North Atlantic Oscillation influence on Europe: climate impacts and associated physical mechanisms, Clim. Res., 20, 9–17, https://doi.org/10.3354/cr020009, 2002.

Trigo, R. M., Pozo-Vázquez, D., Osborn, T. J., Castro-Díez, Y., Gámiz-Fortis, S., and Esteban-Parra, M. J.: North Atlantic Oscillation influence on precipitation, river flow and water resources in the Iberian Peninsula, Int. J. Climatol., 24, 925–944, https://doi.org/10.1002/joc.1048, 2004.

Trouet, V., Esper, J., Graham, N. E., Baker, A., Scourse, J. D., and Frank, D. C.: Persistent positive North Atlantic Oscillation mode dominated the Medieval Climate Anomaly, Science, 324, 78–80, https://doi.org/10.1126/science.1166349, 2009.

Vansteenberge, S., de Winter, N. J., Sinnesael, M., Verheyden, S., Goderis, S., Van Malderen, S. J. M., Vanhaecke, F., and Claeys, P.: Reconstructing seasonality through stable-isotope and trace-element analyses of the Proserpine stalagmite, Han-sur-Lesse Cave, Belgium: indications for climate-driven changes during the last 400 years, Clim. Past, 16, 141–160, https://doi.org/10.5194/cp-16-141-2020, 2020.

Vicente-Serrano, S. M., González-Hidalgo, J. C., de Luis, M., and Raventós, J.: Drought patterns in the Mediterranean area: the Valencia region (eastern Spain), Clim. Res., 26, 5–15, https://doi.org/10.3354/cr026005, 2004.

Vicente-Serrano, S. M.: Spatial and temporal analysis of droughts in the Iberian Peninsula (1910–2000), Hydrol. Sci. J., 51, 83–97, https://doi.org/10.1623/hysj.51.1.83, 2006.

Voarintsoa, N. R. G., Railsback, L. B., Brook, G. A., Wang, L., Kathayat, G., Cheng, H., Li, X., Edwards, R. L., Rakotondrazafy, A. F. M., and Madison Razanatseheno, M. O.: Three distinct Holocene intervals of stalagmite deposition and nondeposition revealed in NW Madagascar, and their paleoclimate implications, Clim. Past, 13, 1771–1790, https://doi.org/10.5194/cp-13-1771-2017, 2017.

Wassenburg, J. A., Immenhauser, A., Richter, D. K., Jochum, K. P., Fietzke, J., Deininger, M., ... and Sabaoui, A.: Climate and cave control on Pleistocene/Holocene calcite-to-aragonite transitions in speleothems from Morocco: Elemental and isotopic evidence, Geochim. Cosmochim. Acta, 92, 23–47, https://doi.org/10.1016/j.gca.2012.06.002, 2012.

Wirth, S. B., Glur, L., Gilli, A., and Anselmetti, F. S.: Holocene flood frequency across the Central Alps: solar forcing and evidence for variations in North Atlantic atmospheric circulation, Quaternary Sci. Rev., 80, 112–128, https://doi.org/10.1016/j.quascirev.2013.09.002, 2013.

Wong, C. I., Banner, J. L., and Musgrove, M.: Seasonal dripwater Mg/Ca and Sr/Ca variations driven by cave ventilation: Implications for and modeling of speleothem paleoclimate records, Geochim. Cosmochim. Acta, 75, 3514–3529, https://doi.org/10.1016/j.gca.2011.03.025, 2011.

Wynn, P. M., Fairchild, I. J., Borsato, A., Spötl, C., Hartland, A., Baker, A., Frisia, S., and Baldini, J. U. L.: Sulphate partitioning into calcite: Experimental verification of pH control and application to seasonality in speleothems, Geochim. Cosmochim. Acta, 226, 69–83, https://doi.org/10.1016/j.gca.2018.01.020, 2018.

Zhou, H., Wang, Y., Huang, L., and Mai, S.: Speleothem Mg, Sr and Ba records during the MIS 5c-d, and implications for paleoclimate change in NE Sichuan, Central China, Chin. Sci. Bull., 56, 3445–3450, https://doi.org/10.1007/s11434-011-4681-y, 2011.

https://doi.org/10.5194/egusphere-2026-3717
Preprint. Discussion started: 7 July 2026

1107 Zimmerman, R. W., Chen, G., Hadgu, T., and Bodvarsson, G. S.: A numerical dual-porosity model with semianalytical
1108 treatment of fracture/matrix flow, Water Resour. Res., 29, 2127–2137, https://doi.org/10.1029/93WR00749, 1993.